

# Compressed Sensing for Surface Characterization and Metrology

Jianwei Ma

**Abstract**—Surface metrology is the science of measuring small-scale features on surfaces. In this paper, a novel compressed sensing (CS) theory is introduced for the surface metrology to reduce data acquisition. We first describe that the CS is naturally fit to surface measurement and analysis. Then, a geometric-wavelet-based recovery algorithm is proposed for scratched and textural surfaces by solving a convex optimal problem with sparse constrained by curvelet transform and wave atom transform. In the framework of compressed measurement, one can stably recover compressible surfaces from incomplete and inaccurate random measurements by using the recovery algorithm. The necessary number of measurements is far fewer than those required by traditional methods that have to obey the Shannon sampling theorem. The compressed metrology essentially shifts online measurement cost to computational cost of offline nonlinear recovery. By combining the idea of sampling, sparsity, and compression, the proposed method indicates a new acquisition protocol and leads to building new measurement instruments. It is very significant for measurements limited by physical constraints, or is extremely expensive. Experiments on engineering and bioengineering surfaces demonstrate good performances of the proposed method.

**Index Terms**—Compressed sensing (CS)/compressive sampling, curvelets, incomplete measurement, sparse recovery, surface characterization, surface metrology, wave atoms.

## I. INTRODUCTION

ENGINEERING surfaces are composed of multiscale topographies, e.g., roughness, waviness, form errors, random ridges/valleys, and peaks/pits. The functional topographical features impact directly on the mechanical and physical properties of the whole system, such as wear, friction, lubrication, corrosion, fatigue, coating, and paintability in many disciplines, including tribology, fluid mechanics, optics, semiconductors, microelectronics, manufacturing, biology, and medicine. For instance, during the functional operation of interacting surfaces, peaks and ridges act as sites of high contact stress and abrasion, whereas the pits, valleys, and scratches (i.e., polish line or line-like wear) affect the lubrication and fluid retention properties. Surfaces also play a vital role in biology and medicine with most biological reactions occurring

Manuscript received March 5, 2008; revised May 4, 2009. This work was supported by the National Natural Science Foundation of China under Contract 40704019 and the Tsinghua Basic Research Fund under Contract JC2007030. The Associate Editor coordinating the review process for this paper was Dr. Emil Petriu.

The author is with the School of Aerospace, Tsinghua University, Beijing 100084, China, and also with the Centre de Geosciences, Ecole des Mines de Paris, 77305 Fontainebleau, France (e-mail: jma@tsinghua.edu.cn).

Color versions of one or more of the figures in this paper are available online at <http://ieeexplore.ieee.org>.

Digital Object Identifier 10.1109/TIM.2009.2027744

on surfaces and interfaces, *in vivo*. Surface metrology has also been used to support scientific discoveries in a variety of fields, including anthropology, archeology, geology, and biochemistry. Therefore, a highly accurate measurement, characterization, and metrology is an important issue for corresponding functional analysis [28], [29], [32], [33], [50].

Multiple methods were implemented to measure different characteristics, including engineering surfaces [50]. Methods including scan, ultrasonics, and scatter have also been developed. For instance, the metrological freak diffractometer based on the scattering method images the source in the Fourier transform plane: speckle techniques and holographic techniques for roughness measurement. Recent instruments including scanning electron microscope (SEM), scanning tunneling microscope, atomic force microscope, magnetic force microscopy, computer tomography (CT), and magnetic resonance imaging (MRI) have largely improved part of restrictions of conventional methods for different physical and medical applications. The versatility of instruments has allowed many different surface experiments to be carried out. These include the measurement and detection of growth in biological specimens, the initiation of some chemical reactions, the machining of substrates, and the microfabrication and movement of material around the surface.

All the aforementioned methods fall into direct measuring (e.g., stylus methods measure the roughness in space domain) and indirect measuring (e.g., CT and MRI collect data in the radon and Fourier transform domains, respectively). We propose here another approach named compressed measurement.

The traditional strategy of surface characterization (denoising, compression, feature extraction, etc.) and metrology requires exact measurements of full surface, computation of the complete set of filtering coefficients, selection of the significant coefficients, and reconstruction of these coefficients to get a required surface [28], [29], [32], [33]. Most existing methods for surface characterization and metrology follow this rule. However, very often, the number of measuring sensors may be limited by physical constraints, the measurements may be extremely expensive, or the sensing process may be slow so that one can only measure the object for a few times. The traditional strategy is extremely wasteful of the massive data acquisition and measuring time. Therefore, many researchers are seeking for methods of how one can reduce the amount of acquired data without degrading the metrology quality.

A novel theory named compressed sensing (CS) or compressive sampling has been proposed by Candès *et al.* [5]–[8] and Donoho [20] to answer the question of data acquisition. The basic principle of CS is that sparse or compressible

signals can be reconstructed from a surprisingly small set of measurements. Different from the classical Shannon sampling theorem or Nyquist rate, the sampling rate must be at least twice the maximum frequency presented in the signals; the CS says that one can recover certain signals from far fewer measurements than traditional methods use if the signals themselves are compressible. The term ‘‘compressible’’ means that the signals are sparse or transformed sparse, i.e., there are only very limited pixels or transformed coefficients with nonzero values. Actually, most natural and real-life surfaces are compressible in some fixed transforms such as discrete cosine transform, wavelet transform [14], [26], curvelet transform [11], [12], and wave atom transform [17]. A few potential applications of the CS theorem have been made in compressive imaging, wireless sensing networks, analog-to-information conversion, biosensing for deoxyribonucleic acid microarrays, etc. For details, we refer readers to several review papers [2], [9], [10].

Roughly speaking, if surfaces exhibit transform sparsity, and if incomplete measurements result in incoherent artifacts in the transform domain, then the surfaces can be recovered from the incomplete measurement by appropriate nonlinear recovery methods. In particular, if one measures linear combinations of Fourier coefficients (called  $K$ -space measurement blow), CS claims that the real surfaces can be accurately reconstructed from a small measured subset of  $K$ -space, rather than an entire  $K$ -space. In this paper, based on directional wavelet frames, we apply the idea of CS to surface metrology, renamed compressed measurement or compressed metrology, which directly concerns geometric and structural features instead of pixel’s information of surfaces.

The CS theory requires the following three aspects.

- 1) The desired surfaces are compressible, i.e., they have sparse representation in a known transform domain. In fact, real surfaces are naturally compressible in an appropriate transform. Here, we mainly care about the surfaces with scratches that are sparse in the curvelet transform domain and the surfaces with textures that are sparse in the wave atom domain.
- 2) The measurement matrices should be noise-like incoherent/uncorrelative to the sparse transforms. Normally, the measurement matrices can be taken as random matrices that are incoherent to almost all sparse transforms. CS combines the idea of sampling and compression, which can lead to build simpler and cheaper measurement instruments for metrology in many fields. How the measuring matrices are designed would indicate a design of new measurement instruments.
- 3) A nonlinear CS recovery algorithm, particularly an iterative curvelet/wave atom thresholding, is applied by solving a convex-optimization problem with sparse constrains.

It should be emphasized that the theme in this paper is totally different from our previous work in [32], [33], [35], and [36]. In previous work, we focus on surface sparse representation and feature extraction using sparse transforms. In this paper, we focus on imaging or measurement mechanism by apply-

ing a new mathematical theory named CS. The compressed-sensing measurement includes the following two steps: 1) on-line encoding measurement and 2) offline decoding recovery. In the offline recovery step, we also need to use some sparse transforms to build a sparse-promoting nonlinear recovery algorithm. In this paper, the sparse transforms are hired by an iterative thresholding framework for compressed-sensing recovery, instead of feature extraction. The sparse representation by curvelets and wave atoms addressed in previous papers [35], [36] can be seen as prior knowledge in the compressed-sensing measurement.

In the remainder of this paper, we first introduce the CS theory from the point of view of mathematics in Section II. In Section III, we describe that the curvelet transform and wave atom transform naturally fit for sparse representation of textural surfaces. Surfaces can be recovered stably by the proposed iterative curvelet and wave atom thresholding described in Section IV. Experiments on the compressed measurement for various surfaces are given in Section V. Finally, conclusions and a few new directions are drawn in Section VI.

## II. ENCODE: COMPRESSED MEASUREMENT

CS handles a fundamental problem of recovering a finite signal  $x$  from a limited set of random measurements  $y$ . This theory indicates that one can only do part of random measurements of engineering surfaces, instead of high-density measurements limited by the Shannon sampling theorem, to carry out highly accurate metrology. Let  $\Phi \in \mathcal{C}^{K,N}$ ,  $K \ll N$  be a so-called CS measurement matrix. Typical examples of the measurement matrices are Fourier transform  $F$  followed by a random undersampling operator  $R$ . The problem can be described as [6], [8]

$$y = \Phi x + \epsilon = R F x + \epsilon. \quad (1)$$

Here,  $\epsilon$  denotes the possible measurement errors or noise. Most of the time,  $x$  is not sparse in the space domain but is sparse in the transform domain by a basis  $\Psi$  (i.e.,  $x$  is transform sparse or compressible if the most coefficients concentrate near zeros). In this case, one can write (1) as

$$y = \Phi \Psi \vartheta + \epsilon. \quad (2)$$

To recover the sparse coefficient  $\vartheta$ , one solves an optimization problem by constructing the following cost function to be minimized:

$$\min_{\vartheta} \left\{ \|y - \tilde{A} \vartheta\|^2 + \lambda \sum_i^N p(|\vartheta_i|) \right\}, \quad \tilde{A} = \Phi \Psi. \quad (3)$$

Here, the first term denotes preserving information by measuring how close the decoding solution is to the input information. The second term is a regularization that represents *a priori* sparse information of original signals. The  $p$  is a function of  $\vartheta$ , and  $\lambda$  is a positive constant that determines the importance of the regularization term. This problem can also be solved

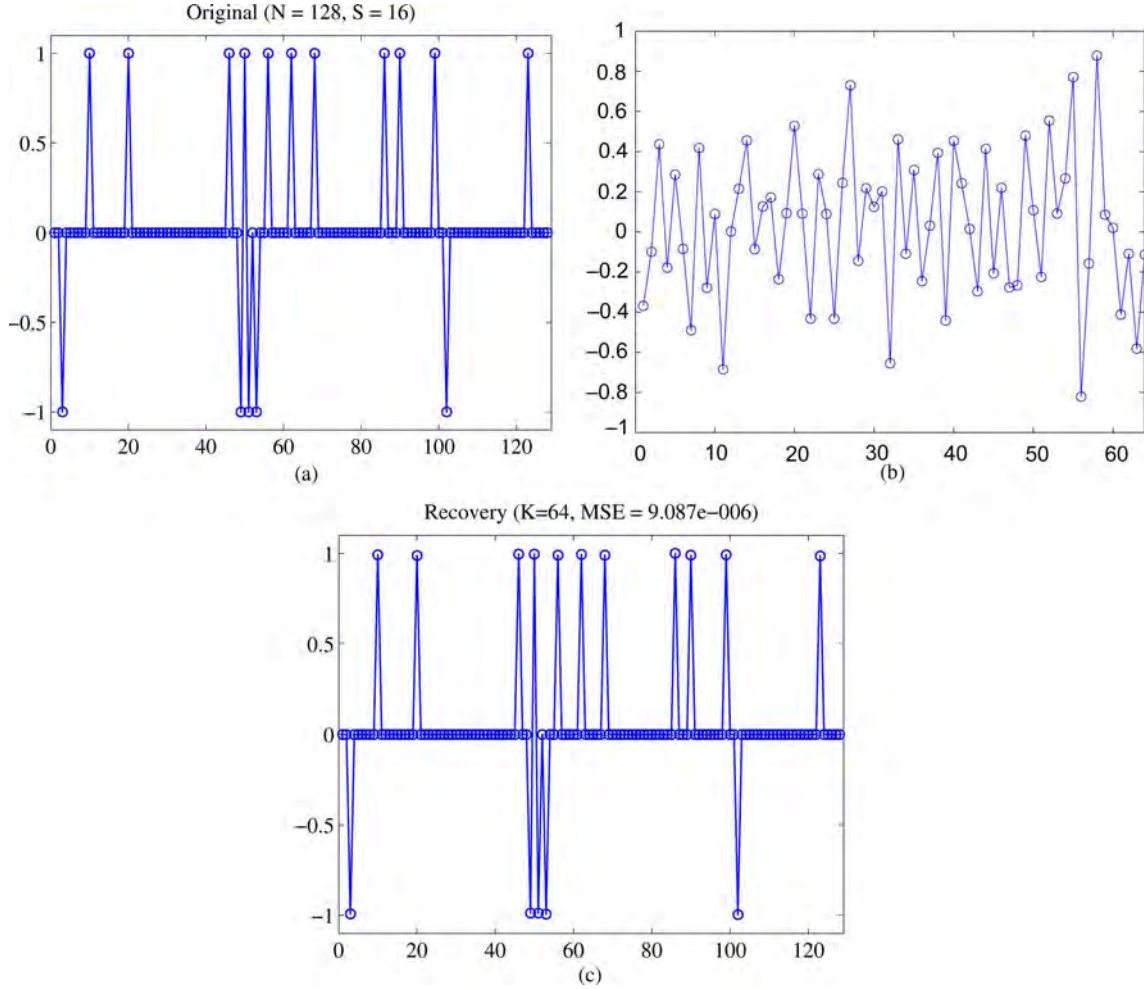


Fig. 1. One-dimensional sample for compressed sensing. (a) Original unknown signal. (b) Randomly measured signal. (c) Recovered signal by compressed sensing. The horizontal coordinate denotes sampling point, and the vertical coordinate denotes amplitude of the signal.

by  $l_1$ -minimization, which is also known as basis pursuit with inequality constraints and is described by [6]

$$\min_{\vartheta} \|\vartheta\|_{l_1}, \quad \text{subject to } \|\tilde{A}\vartheta - y\|_{l_2} \leq \epsilon. \quad (4)$$

If without considering the noise  $\epsilon$ , the convex optimization problem is a linear programming known as basis pursuit [5], which is given by

$$\min_{\vartheta} \|\vartheta\|_{l_1}, \quad \text{subject to } \tilde{A}\vartheta = y. \quad (5)$$

It seems hopeless to solving the underdetermined equations since the rows are much fewer than the columns in  $\tilde{A}$ . However, the CS has told us that if the signal  $x$  is sparse or compressible, the underdetermined system of equations can be exactly solved. Supposing that there are  $S$  nonzero coefficients (i.e., so-called  $S$ -sparse,  $\|\vartheta\|_{l_0} = S \ll N$ ), one just needs measurement numbers  $K$  in Fourier space with frequencies selected randomly, satisfying

$$K \geq C \cdot S \cdot \log N. \quad (6)$$

Let us first look at a 1-D example to understand the idea of CS. Assume that one has an unknown signal with  $N = 128$  sampling points and  $S = 16$  nonzero values, as shown in

Fig. 1(a). The numbers, positions, and values of the nonzero values are unknown in our experiment. One cannot use such information but can discover this information by the example algorithm. The *a priori* knowledge used is that the signal is sparse in the space domain. For instance, one considers a  $64 \times 128$  measurement matrix  $\Phi$  (i.e.,  $K = 64$ ) assembled by random numbers to measure the 1-D original unknown signal shown in Fig. 1(a). Each measurement, mathematically speaking, equals to an inner product of a row of the measurement matrix and the unknown signal. The measurements can be repeated up to 64 times using the different rows of the measurement matrix. Fig. 1(b) shows the measurement results. The CS says that one can exactly recover the unknown signal from these randomly measurements using nonlinear recovery methods. Fig. 1(c) displays a recovered signal from the incomplete measurements by using a so-called gradient projection for sparse reconstruction (GPSR) method proposed in [24]. The recovered signal is almost the same as original signal (the mean-square error  $\text{MSE} = 9.087e - 006$ ). Of course, for most applications, the usable *a priori* knowledge is the sparsity of signals in the transform domain instead of in the space domain. The surfaces that we handle in this paper are sparse in the curvelet and wave atom domains.

Naturally, the following two basic questions arise: 1) What are good CS matrices and how many measurements are required for successful reconstruction and 2) what are the most efficient decoder or recovery algorithm to solve the optimal problem?

To answer the first question, Candès *et al.* [5], [6] proposed a sufficient condition named restricted isometry property (RIP) for CS matrices. A measurement matrix  $\Phi$  satisfies the RIP of order  $S$  with constant  $\delta_S \in (0, 1)$ , if

$$(1 - \delta_S)\|x\|_{l_2}^2 \leq \|\Phi_T x\|_{l_2}^2 \leq (1 + \delta_S)\|x\|_{l_2}^2, \\ x \in R^N; \quad \|T\| \leq S. \quad (7)$$

Here,  $\Phi_T$ ,  $T \subset 1, \dots, N$ , denotes the  $K \times |T|$  submatrix obtained by extracting the columns of  $\Phi$  corresponding to the indices in  $T$ . The RIP says that the mapping  $\Phi$  acts like an isometry on  $S$ -space vectors. It requires that every set of columns with cardinality less than  $S$  approximately behaves like an orthonormal system. A measurement matrix  $\Phi$  satisfying the RIP ensures the exact and unique recovery to be obtained.

Furthermore, for compressible signals, a good measurement matrix should also be incoherent in the sparse basis. The greater incoherence of the measurement/sparsity pair  $(\Phi, \Psi)$  there is, the smaller the number of measurements will be needed. Supposing that  $\Phi$  is obtained by selecting  $K$  rows uniformly at random from an  $N \times N$  orthonormal matrix and renormalizing the columns so that they are unit normed, one has

$$S \leq C \cdot \frac{1}{v^2} \cdot \frac{K}{(\log N)^4} \quad (8)$$

where  $v := \sqrt{N} \max_{1 \leq i, j \leq N} |\langle \phi_i, \varphi_j \rangle|$  ( $\phi_i \in \Phi$ ,  $\varphi_j \in \Psi$ ) is referred to as the mutual coherent between the measurement basis  $\Phi$  and the sparsity basis  $\Psi$ . Generally,  $v(\Phi, \Psi) \in [1, \sqrt{N}]$ . In particular,  $v = 1$  when  $\Phi$  is the canonical or spike basis  $\phi_m(t) = \delta(t - m)$  and  $\Psi$  is the Fourier basis  $\varphi_j = N^{-1/2} e^{i2\pi jt/N}$ . That is to say, if  $\Phi$  is a partial Fourier matrix obtained by selecting  $K$  rows uniformly at random, we have  $S \leq C \cdot K/(\log N)^4$ . It has been known that noiselet measurement  $\Phi$  and Haar wavelets  $\Psi$  have mutual coherent  $v = \sqrt{2}$ ; noiselet measurement and Daubechies DB4 wavelets have  $v = \sqrt{2.2}$  [9]. Normally, one can choose random measurement matrices, which are largely incoherent to any fixed basis  $\Psi$ . The known CS measurement matrices  $\Phi$  satisfying the RIP are random matrices, including Gaussian, Bernoulli, and random partial bounded orthogonal matrices. Recently, how a deterministic and explicit measurement matrix is constructed has been concerned by De Vore [18] and Indyk [27]. How the design of the measurement matrices that need fewer measurement is optimized was also emphasized by Elad [22].

Assuming that the measurement matrix  $\Phi$  is an identity matrix  $I$  (i.e., without undersampling) and  $\Psi$  is a wavelet transform, the problem in (3) degenerates to the well-known wavelet regularization (see, e.g., [1]). This regularization is closely related to wavelet thresholding. Specifically, if the penalty function is taken as  $l_1$  penalty  $p(|\vartheta|) = |\vartheta|$ , the solution is a wavelet soft-thresholding rule; if the penalty function is given by  $p_\lambda(|\vartheta|) = \lambda^2 - (|\vartheta| - \lambda)^2 I(|\vartheta| < \lambda)$ , the solution is a hard-thresholding rule.

In addition to satisfying the RIP condition, the choice of  $\Phi$  depends on the physics of measurement problem. For example, in the case of scattered field, the electric field integral equations (operator  $\Phi$ ) are used for recovering the scatter geometry (signal  $x$ ) from the randomly incomplete measured scattered field (signal  $y$ ). In this paper, we consider an optical measurement system for frequency  $K$ -space measurements. The prior knowledge that we used in the framework of compressed measurement is that most scratched and textural surfaces can be sparsely represented by a  $\Psi$  called curvelet or wave atom transform. We proposed an iterative curvelet or wave atom thresholding as a nonlinear recovery algorithm for the compressed measurements. Now, the measurement matrix  $\Phi$  is a random sampling of Fourier coefficients of engineering surfaces, and original unknown surfaces or features  $x$  can be recovered from the measurements  $y$  by using the offline iterative thresholding methods. It is also possible to directly reconstruct the wanted features for metrology without the need to recover the full surface. The compressed measurement is a simple and efficient signal acquisition protocol with samples at a low rate and later uses computational power for optimal reconstruction from the incomplete set of measurements. The compressed measurement essentially shifts online measuring cost into offline computational cost of nonlinear recovery. Therefore, this metrology strategy can be called as computational metrology. Many existing sparse transforms and nonlinear optimal algorithms can be incorporated into the compressed measurement for various engineering surfaces.

### III. SPARSITY IN CURVELET AND WAVE ATOM DOMAINS

Sparse transforms have successfully been applied for surface metrology. An early method to be used as a filter is a Gaussian or spline filter. Although it has been widely used in surface metrology, the technique is insufficient in addressing the non-stationary and multiscale nature of rough surfaces. Applications of wavelets on surfaces analysis have become an increasing interest (see, e.g., [13], [28], [29], and [44] among a vast amount of current literature). The main advantages of wavelet-based methods are space–frequency localization and multiscale view of the features of surfaces. Unfortunately, traditional wavelets are not optimal to analyze surfaces with scratches or textures because wavelets ignore geometric properties of edges and textures, which leads to strong oscillating artifacts along the scratches of roughness (see [32]). Recently, Ma *et al.* [32]–[36] proposed a series of so-called artifact-free characteristic methods based on geometric wavelets. In particular, ridgelets, curvelets, and wave atoms have been applied to extract straight scratches, curve scratches, and textures from surfaces, respectively. It should also be noted that from another way, Brown *et al.* [4] considers the multiscale metrology by using a so-called scale-sensitive fractal analysis, which was recently used to characterize dental microwear textures in fossil hominid to understand the diets and evolution of our lineages [46]. However, the use of sparsity in inverse problems on data recovery is the most recent step.

Following the previous work on sparse representation of surfaces based on curvelets and wave atoms, we extend these

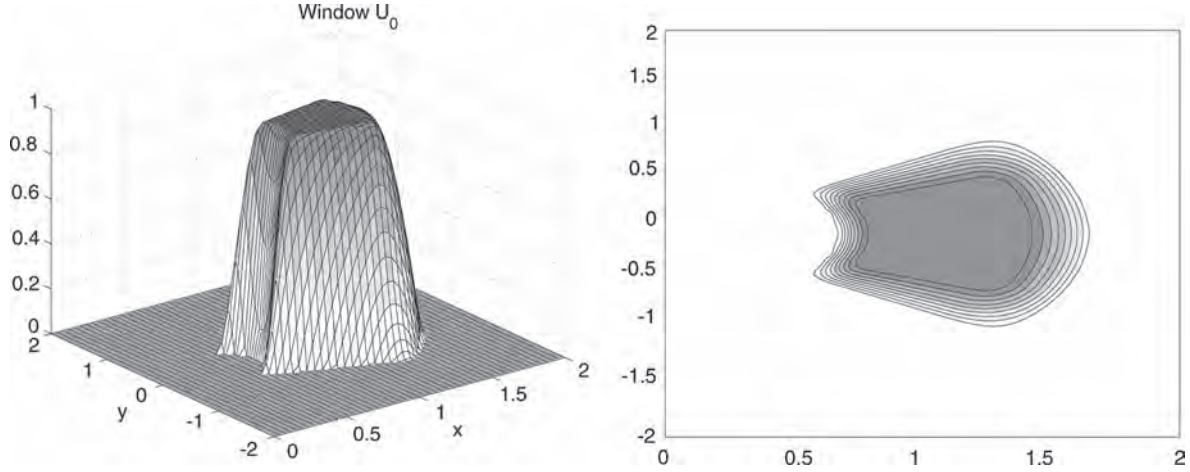


Fig. 2. (left) Window  $U_0(\xi)$ . (right) Its support.

sparse transforms to compressed measurement, which is a special inverse problem on recovery of incomplete data.

### A. Curvelets for Surfaces With Scratches

Curvelet transform allows an optimal sparse representation of objects with  $C^2$  singularities. The needle-shape elements of this transform own very high directional sensitivity and anisotropy. For a smooth object  $f$  with discontinuities along smooth curves, the best  $m$ -term approximation  $\tilde{f}_m$  by curvelet thresholding obeys  $\|f - \tilde{f}_m\|_2^2 \leq Cm^{-2}(\log m)^3$ , while for wavelets, the decay rate is only  $m^{-1}$ . Surprising performance has been shown in the fields of image processing, see, e.g., [35], [37], [38], [47]. It essentially obeys a parabolic scaling law between the width and length of an element (width  $\approx$  length<sup>2</sup>) and directional sensitivity (orientations =  $1/\sqrt{\text{scale}}$ ). See Fig. 1 (left) for an example of curvelet elements. Thus, it is good to characterize surfaces with general scratches. Several curvelet-like geometric multiscale transform, e.g., bandlets [43] and contourlets [19], have also been proposed to restore the curve singularities in a different way.

In the following, we give an outline for the second-generation discrete curvelet transform (DCuT) [11], [12], which is considerably simpler to use than the original first-generation formulation based on the block ridgelet transform. The second-generation DCuT is implemented by means of special frequency-window partitions. For details on curvelets, we refer to recent review papers [39], [40].

Let  $V(t)$  and  $W(r)$  be a pair of smooth nonnegative real-valued window functions such that  $V$  is supported on  $[-1, 1]$  and  $W$  on  $[1/2, 2]$ . The windows satisfy the admissibility conditions  $\sum_{l=-\infty}^{\infty} V^2(t-l) = 1$ ,  $t \in \mathbb{R}$ ,  $\sum_{j=-\infty}^{\infty} W^2(2^{-j}r) = 1$ ,  $r > 0$ . These conditions are satisfied, taking, e.g., the scaled Meyer windows [38], i.e.,

$$V(t) = \begin{cases} 1, & |t| \leq 1/3 \\ \cos \left[ \frac{\pi}{2} \nu(3|t| - 1) \right], & 1/3 \leq |t| \leq 2/3 \\ 0, & \text{else} \end{cases}$$

$$W(r) = \begin{cases} 1, & 5/6 \leq r \leq 4/3 \\ \cos \left[ \frac{\pi}{2} \nu(5 - 6r) \right], & 2/3 \leq r \leq 5/6 \\ \cos \left[ \frac{\pi}{2} \nu(3r - 4) \right], & 4/3 \leq r \leq 5/3 \\ 0, & \text{else} \end{cases}$$

where  $\nu$  is a smooth function satisfying

$$\nu(x) = \begin{cases} 0, & x \leq 0 \\ 1, & x \geq 1 \end{cases}, \quad \nu(x) + \nu(1-x) = 1; \quad x \in \mathbb{R}.$$

Let the Fourier transform of  $f \in L^2(\mathbb{R}^2)$  be defined by  $\hat{f}(\xi) := (1/2\pi) \int_{\mathbb{R}^2} f(x) e^{-i(x,\xi)} dx$ . Now, for  $j \geq 0$ , let the window  $U_j(\xi)$ ,  $\xi = (\xi_1, \xi_2) \in \mathbb{R}^2$  in the frequency domain be given by

$$U_j(\xi) = 2^{-3j/4} W(2^{-j}|\xi|) V(2^{\lfloor j/2 \rfloor} \theta), \quad \xi \in \mathbb{R}^2$$

where  $(|\xi|, \theta)$  denotes the polar coordinates corresponding to  $\xi$ . The support of  $U_j$  is a polar wedge determined by  $\text{supp } W(2^{-j}\cdot) = [2^{j-1}, 2^{j+1}]$  and  $\text{supp } V(2^{\lfloor j/2 \rfloor}\cdot) = [-2^{-\lfloor j/2 \rfloor}, 2^{-\lfloor j/2 \rfloor}]$ . Fig. 2 shows an example of the window  $U_0$  and its support [38].

The system of curvelets is now indexed by the following three parameters: 1) a scale  $2^{-j}$ ,  $j \in \mathbb{N}_0$ ; 2) an equispaced sequence of rotation angles  $\theta_{j,l} = 2\pi l \cdot 2^{-\lfloor j/2 \rfloor}$ ,  $0 \leq l \leq 2^{\lfloor j/2 \rfloor} - 1$ ; and 3) a position  $x_k^{(j,l)} = R_{\theta_{j,l}}^{-1}(k_1 2^{-j}, k_2 2^{-\lfloor j/2 \rfloor})^T$ ,  $(k_1, k_2) \in \mathbb{Z}^2$ , where  $R_{\theta_{j,l}}$  denotes the rotation matrix with angle  $\theta_{j,l}$ . The curvelets are defined by

$$\varphi_{j,l,k}(x) := \varphi_j \left( R_{\theta_{j,l}} \left( x - x_k^{(j,l)} \right) \right), \quad x = (x_1, x_2) \in \mathbb{R}^2$$

where  $\hat{\varphi}_j(\xi) := U_j(\xi)$ , i.e.,  $U_j$  is the Fourier transform of  $\varphi_j$ . Observe that in the spatial domain,  $\varphi_{j,l,k}$  rapidly decays outside of a  $2^{-j}$  by  $2^{-j/2}$  rectangle with center  $x_k^{(j,l)}$  and orientation  $\theta_{j,l}$  with respect to the vertical axis (see Fig. 3). Fig. 4 shows the support of windows at different scales and orientations. The wedges are longer and thinner with growing  $j$ . Corresponding to the time domain, curvelets have a well-localized needle-shaped form.

For simplification, let  $\mu = (j, l, k)$  be the collection of the triple index. The system of curvelets  $(\varphi_\mu)$  forms a tight frame in  $L^2(\mathbb{R}^2)$ , i.e., each function  $f \in L^2(\mathbb{R}^2)$  can be represented by

$$f = \sum_{\mu} c_{\mu}(f) \varphi_{\mu}.$$

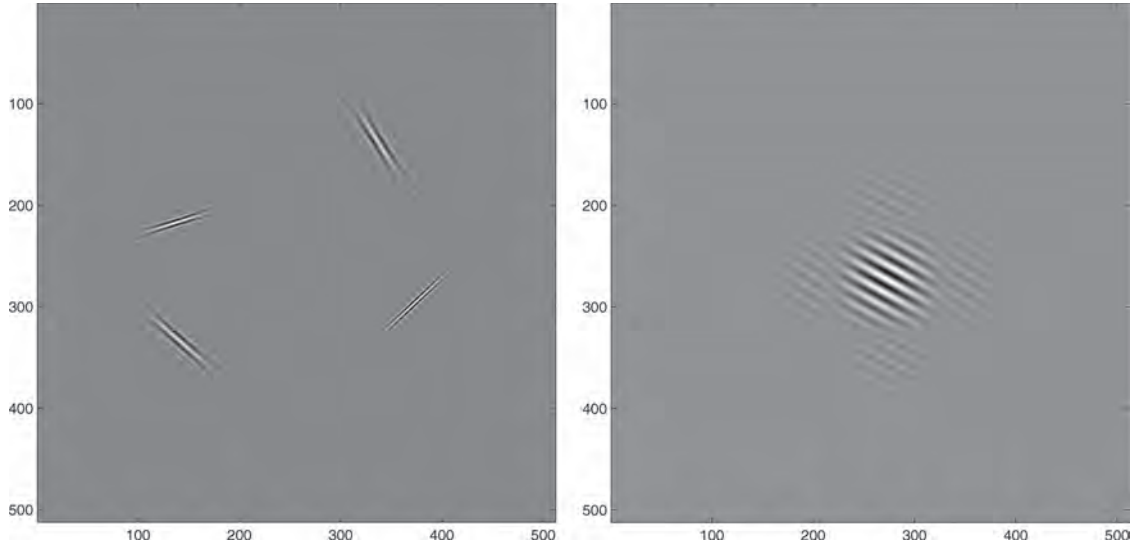


Fig. 3. Elements of (left) curvelets and (right) wave atoms in the spatial domain.

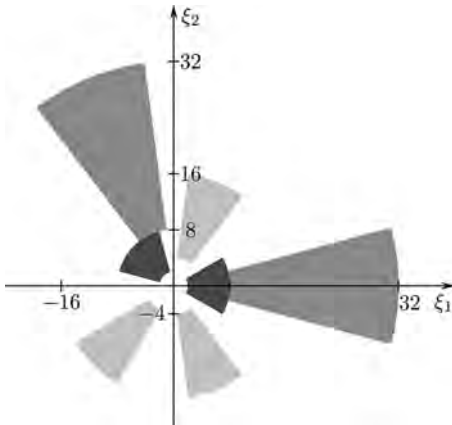


Fig. 4. Supports of frequency windows for (dark grey)  $\varphi_{2,0,k}$  and  $\varphi_{2,5,k}$ , (light grey)  $\varphi_{3,3,k}$ ,  $\varphi_{3,6,k}$  and  $\varphi_{3,13,k}$ , and (grey)  $\varphi_{4,0,k}$  and  $\varphi_{4,11,k}$ .

Using Parseval's identity, the curvelet coefficients are given by

$$\begin{aligned} c_\mu(f) &:= \langle f, \varphi_\mu \rangle = \int_{\mathbb{R}^2} \hat{f}(\xi) \overline{\hat{\varphi}_\mu(\xi)} d\xi \\ &= \int_{\mathbb{R}^2} \hat{f}(\xi) U_j(R_{\theta_{j,l}} \xi) e^{i \langle x_k^{(j,l)}, \xi \rangle} d\xi. \end{aligned} \quad (9)$$

The algorithm of forward 2-D DCuT is given as follows.

- 1) Apply a 2-D fast Fourier transform (FFT) to compute the Fourier coefficients  $\hat{f}$  of  $f$ .
- 2) Compute the product  $\hat{f}U_j$ .
- 3) Apply the inverse 2-D FFT to obtain the discrete coefficients  $c_\mu(f)$ .

The forward and inverse DCuTs have the same computational cost of  $\mathcal{O}(N^2 \log N)$  for an  $(N \times N)$  image. The redundancy of the curvelet transform is about 2.8 when wavelets are chosen at the finest scale, and 7.2 otherwise (see, e.g., [12]).

### B. Wave Atoms for Surfaces With Oriented Textures

However, curvelets are not optimal for oscillatory textures; thus, they are not good to characterize surfaces with oriented

textures, e.g., engineering surfaces by grinding, milling, polishing, and honing.

Very recently, Demanet and Ying [17] introduced the so-called wave atoms, which are a variant of 2-D wavelet packets and obey the parabolic scaling of curvelets (see Fig. 3, right). The warped oscillatory functions or oriented textures have a significantly sparser expansion in wave atoms than in other fixed standard representations like Gabor filters, wavelets, and curvelets. The texture-shape elements of wave atoms capture not only the coherence of the pattern along the oscillations like curvelets, but also the pattern across the oscillations. Fig. 3 shows the difference between the elements of the curvelets and wave atoms. The texture-shape elements of wave atoms also own very high directional sensitivity and anisotropy. Obviously, it is natural to apply the wave atoms for characterization of surfaces with oriented textures.

Let us define wave atoms as  $\varphi_\mu(x)$ , with the subscript  $\mu = (j, m, n) = (j, m1, m2, n1, n2)$  indexing a phase-space point  $(x_\mu, \omega_\mu)$  by  $x_\mu = 2^{-j}n$ ,  $\omega_\mu = \pi 2^j m$ ,  $C_1 2^j \leq \max_{i=1,2} |m_i| \leq C_2 2^j$ , where  $C_1$  and  $C_2$  are two positive constants. Then, the elements of a frame of wave packets  $\varphi_\mu$  are called wave atoms when

$$\begin{aligned} |\tilde{\varphi}_\mu(\omega)| &\leq C_M \cdot 2^{-j} (1 + 2^{-j} |\omega - \omega_\mu|)^{-M} \\ &\quad + C_M \cdot 2^{-j} (1 + 2^{-j} |\omega + \omega_\mu|)^{-M} \end{aligned} \quad (10)$$

$$|\varphi_\mu(x)| \leq C_M \cdot 2^j (1 + 2^j |x - x_\mu|)^{-M}, \quad M > 0. \quad (11)$$

The oscillations within the envelope of a wave atom in  $x$  have a wavelength  $\sim 2^{-2j}$ .

Let  $g$  be a real-valued continuous function with support included in  $[-7\pi/6, 5\pi/6]$  and such that for  $|\omega| \leq \pi/3$ ,  $g((\pi/2) - \omega)^2 + g((\pi/2) + \omega)^2 = 1$  and  $g(-(\pi/2) - 2\omega) = g((\pi/2) + \omega)$ . Define  $v$  as the inverse Fourier transform  $v(t) = (2\pi)^{-1} \int g(\omega) e^{i\omega t} d\omega$ , and

$$\psi_m^0(t) = 2Re \left\{ e^{i\pi(m+\frac{1}{2})t} v \left( (-1)^n \left( t - \frac{1}{2} \right) \right) \right\}. \quad (12)$$

The Fourier transform of  $\psi_m^0$  is given by [17], [49]

$$\hat{\psi}_m^0(\omega) = e^{-i\omega/2} \left[ e^{i\alpha_m} g \left( \epsilon_m \left( \omega - \pi \left( m + \frac{1}{2} \right) \right) \right) + e^{-i\alpha_m} g \left( \epsilon_{m+1} \left( \omega + \pi \left( m + \frac{1}{2} \right) \right) \right) \right]. \quad (13)$$

Here,  $\epsilon_m = (-1)^m$ ,  $\alpha_m = (\pi/2)(m + (1/2))$ , and  $\sum_m |\hat{\psi}_m^0(\omega)|^2 = 1$ .

Write basis functions as  $\psi_{m,n}^j(x) = \psi_m^j(x - 2^{-j}n) = 2^{j/2} \psi_m^0(2^j x - n)$ . Then, coefficients of the transform can be obtained by

$$c_{j,m,n} = \int \psi_{m,n}^j(x) f(x) dx = \frac{1}{2\pi} \int e^{i2^{-j}n\omega} \overline{\hat{\psi}_m^j(\omega)} \hat{f}(\omega) d\omega. \quad (14)$$

Assuming that the function is discretized at  $x_k = kh$ ,  $h = 1/N$ ,  $k = 1, \dots, N$ , we have

$$c_{j,m,n} \simeq \frac{1}{2\pi} \sum_{k=2\pi(-N/2+1:1:N/2)} e^{i2^{-j}nk} \overline{\hat{\psi}_m^j(k)} \hat{f}(k). \quad (15)$$

The 2-D extension can be formed by the following products:

$$\begin{aligned} \varphi_\mu^+(x_1, x_2) &= \psi_{m_1}^k(x_1 - 2^{-j}n_1) \psi_{m_2}^k(x_2 - 2^{-j}n_2) \\ \varphi_\mu^-(x_1, x_2) &= H\psi_{m_1}^k(x_1 - 2^{-j}n_1) H\psi_{m_2}^k(x_2 - 2^{-j}n_2) \end{aligned}$$

where  $H$  is the Hilbert transform. The combinations  $\varphi_\mu^{(1)} = (\varphi_\mu^+ + \varphi_\mu^-)/2$  and  $\varphi_\mu^{(2)} = (\varphi_\mu^+ - \varphi_\mu^-)/2$  form the wave atom frame and be denoted jointly as  $\varphi_\mu$  [17].

The algorithm can be implemented by the following three steps: 1) Apply 2-D FFT for  $f(x_k)$ ; 2) wrap the product  $\hat{\psi}_m^j \hat{f}$  by periodicity inside the interval  $[-2^j\pi, 2^j\pi]$  for each  $(j, m)$ ; and 3) perform the inverse 2-D FFT. The computational complexity of wave atom transform is  $\mathcal{O}(N^2 \log N)$ .

#### IV. DECODE: NONLINEAR SPARSE RECOVERY

In the last two years, a few iterative algorithms, e.g., orthogonal matching pursuit [48], gradient projection [24], and iterative thresholding algorithms [3], [15], [16], [25], [42], have been proposed by mathematicians to exactly reconstruct the  $x$  in (1) or  $\vartheta$  in (2). In this paper, we follow the way of iterative thresholding since this methodology is considerably robust and simple to be implemented. In particular, the iterative curvelet thresholding and wave atom thresholding are applied for surfaces with scratches and textures, respectively.

Related algorithms on iterative thresholding have been presented for constrained optimization problems by a few researchers (see, e.g., [15], [16], [25], and [42]). For instance, Daubechies *et al.* [15] presented an iterative thresholding algorithm for wavelet regularization (i.e., inverse problem with wavelet sparse constrains). However, in this seminal paper, the problems of undersampling or partial measuring were not considered. Peyré [42] proposed iterative thresholding with best

basis constrains for CS to recover images. We observed that the iterative thresholding is quite related to nonlinear inverse diffusion or the so-called inverse scale space method [51]. We will describe the connections between our proposed method with the inverse diffusion equation elsewhere.

Let us have a look at the motivation of the iterative thresholding for recovery of linear inverse problems. If without undersampling (i.e.,  $\Phi \in \mathcal{C}^{N,N}$ ), one can recover  $x$  by  $x = \Phi^{-1}y - \Phi^{-1}\epsilon$ . Very frequently,  $\Phi$  corresponds to a low-pass filtering so that  $\Phi^{-1}\epsilon$  magnifies the noises, which leads to an ill-posed inverse problem. The iterative thresholding essentially deals with the inverse problem as an iterative denoising. In fact, the iterative thresholding was initially presented as an expectation-maximization algorithm for image deconvolution [24]. Convergence of iterative thresholding algorithm can be found in [15]. The algorithm only requires matrix-vector multiplications of  $\Phi$  and  $\Phi^T$ , and it is based on bounding the matrix  $\Phi^T\Phi$  by a diagonal matrix  $D$  (i.e.,  $D - \Phi^T\Phi$  is positive semidefinite), and thus, the solution of (3) can be obtained by a sequence of simpler denoising. A wide-angle review of iterative thresholding algorithms involving denoising, deconvolution, and CS can be found in [23].

Define the following thresholding function:

$$S_\tau(f, \Psi) = \sum_\mu \tau(c_\mu(f)) \varphi_\mu \quad (16)$$

where  $\tau$  can be taken as a soft-thresholding function defined by a fixed threshold  $\sigma > 0$ , i.e.,

$$\tau_s(x) = \begin{cases} x - \sigma, & x \geq \sigma \\ 0, & |x| < \sigma \\ x + \sigma, & x \leq -\sigma \end{cases}$$

or a hard-thresholding function, i.e.,

$$\tau_h(x) = \begin{cases} x, & |x| \geq \sigma \\ 0, & |x| < \sigma \end{cases}$$

or the continuous garrote thresholding, i.e.,

$$\tau_g(x) := \begin{cases} x - \frac{\sigma^2}{x}, & |x| \geq \sigma \\ 0, & |x| < \sigma \end{cases}$$

which may be a good choice where large coefficients nearly remain unaltered.

By solving a minimization of surrogate function [15], [42], one can obtain the solution by iterating the thresholding function, i.e.,

$$S_\tau(x + \Phi^T(y - \Phi x), \Psi). \quad (17)$$

Outline the algorithm as follows.

- 1) Initialization: set the iterative number  $p = 0$  and initial value  $x_0 = 0$  or a zero-filling reconstruction by interpolating zeros for missed samples [30].
- 2) Update the estimation

$$\tilde{x}_p = x_p + \Phi^T(y - \Phi x_p).$$

3) Apply curvelet/wave atom thresholding for the estimation

$$x_{p+1} = S_{\tau}(\tilde{x}_p, \Psi).$$

- 4) Iteration: if  $\|x_{p+1} - x_p\| > \varepsilon$ , then set  $p + 1$  to  $p$  and go to step 2; otherwise, stop iterations.
- 5) Alternatively, in the last several iterations or after all iterations, one can apply total variation (TV)-synthesis y curvelet/wave atom thresholding [35], [38], which can suppress the pseudo-Gibbs artifacts (small high-frequency oscillatory due to false reconstruction of fine-scale coefficient components) and element-like artifacts while preserving the discontinuous edges and features. Here, the TV of a function  $f$  with  $|\nabla f \in L^1(\Omega)|$  is defined by  $\text{TV}(f) = \int_{\Omega} |\nabla f(\zeta)| d\zeta$  [45]. The thresholding is posed as an optimization problem involving the total variation norm and a constraint on the curvelet space. It can be interpreted as a projected iterative thresholding. Essentially, the TV minimization keeps the significant coefficients unchanged and does not set the insignificant coefficients to zero as conventional shrinkage does but typically makes it optimal small to eliminate the artifacts.

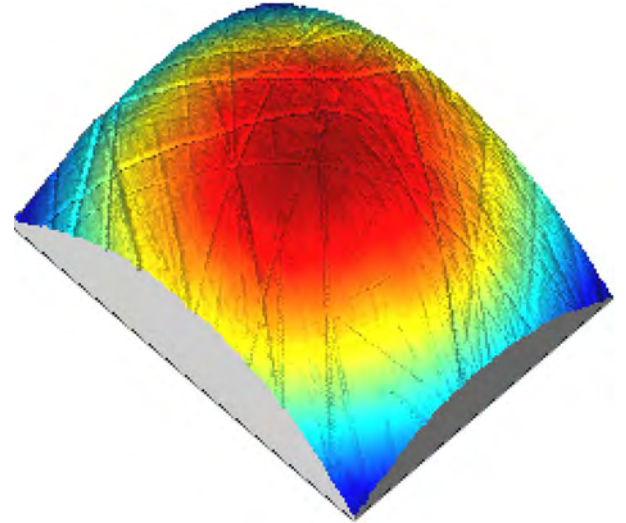
The threshold value  $\sigma$  is dependent on practical problems. The question on how to choose the  $\sigma$  optimally for specific metrology is open. Normally, one can use a uniform threshold value or an updating threshold value through iterations. Recently, the iterative curvelet thresholding has also been applied to deblurring problems with highly incomplete measurements in the field of remote sensing [41].

The iterative thresholding produces a sequence of inverse scale space, which starts from the measurement data (or an initial value with zeros) and approaches the real surfaces as iteration increases. If we use linear decaying threshold values, the produced recovery sequence changes from smooth space to fine space. If the iteration is stopped at a suitable time, large-scale features may already be incorporated into the reconstruction, while fine-scale features are still missing.

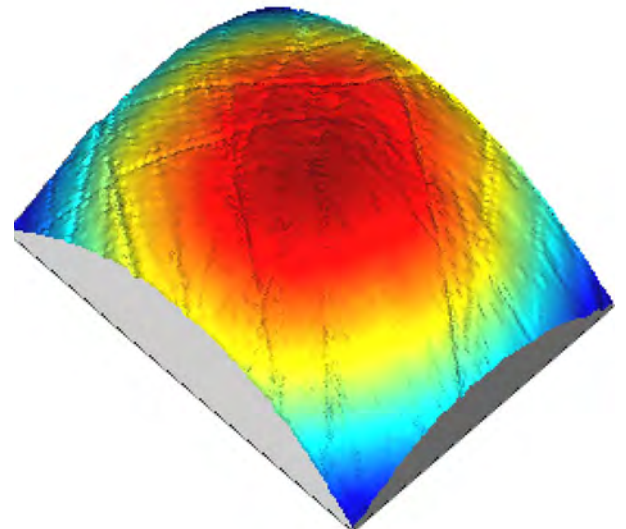
It should be noted that one can apply orthogonal wavelets in this framework for surfaces with point features. A nonlinear conjugate gradient has been used for such a wavelet case in medical magnetic resonance imaging [30].

## V. NUMERICAL EXPERIMENTS

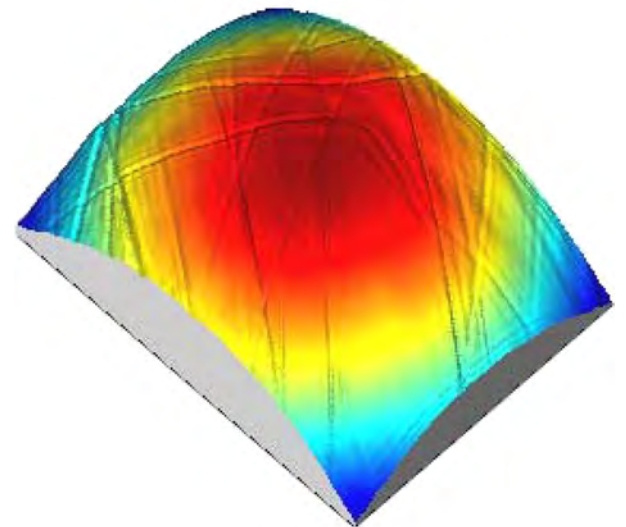
Real surfaces are naturally compressible by suitable coding in an appropriate transform domain. For example, surfaces with peaks/pits are sparse in the wavelet domain, and surfaces with straight scratches are compressible in the ridgelet domain [34], while surfaces with curve scratches have better compressible in the curvelet domain. So far, the sparse representation and decomposition of engineering surfaces has been addressed much in the literature (see, e.g., [13], [28], [29], [32], [34]–[36], and [44]). Fig. 5(a) shows a typical example: a worn metallic femoral head of biomedical orthopedic implant. This surface has a sparse representation in the wavelet frame domain. Fig. 5(b) and (c) presents the partial reconstruction using the largest 1% wavelet and curvelet coefficients. The



(a)



(b)



(c)

Fig. 5. Partially sparse reconstruction of a raw surface topography measured from a metallic joint head implant. (a) Original surface. (b) Reconstructed surface by 1% largest wavelet coefficients. (c) Reconstructed surface by 1% largest curvelet coefficients.

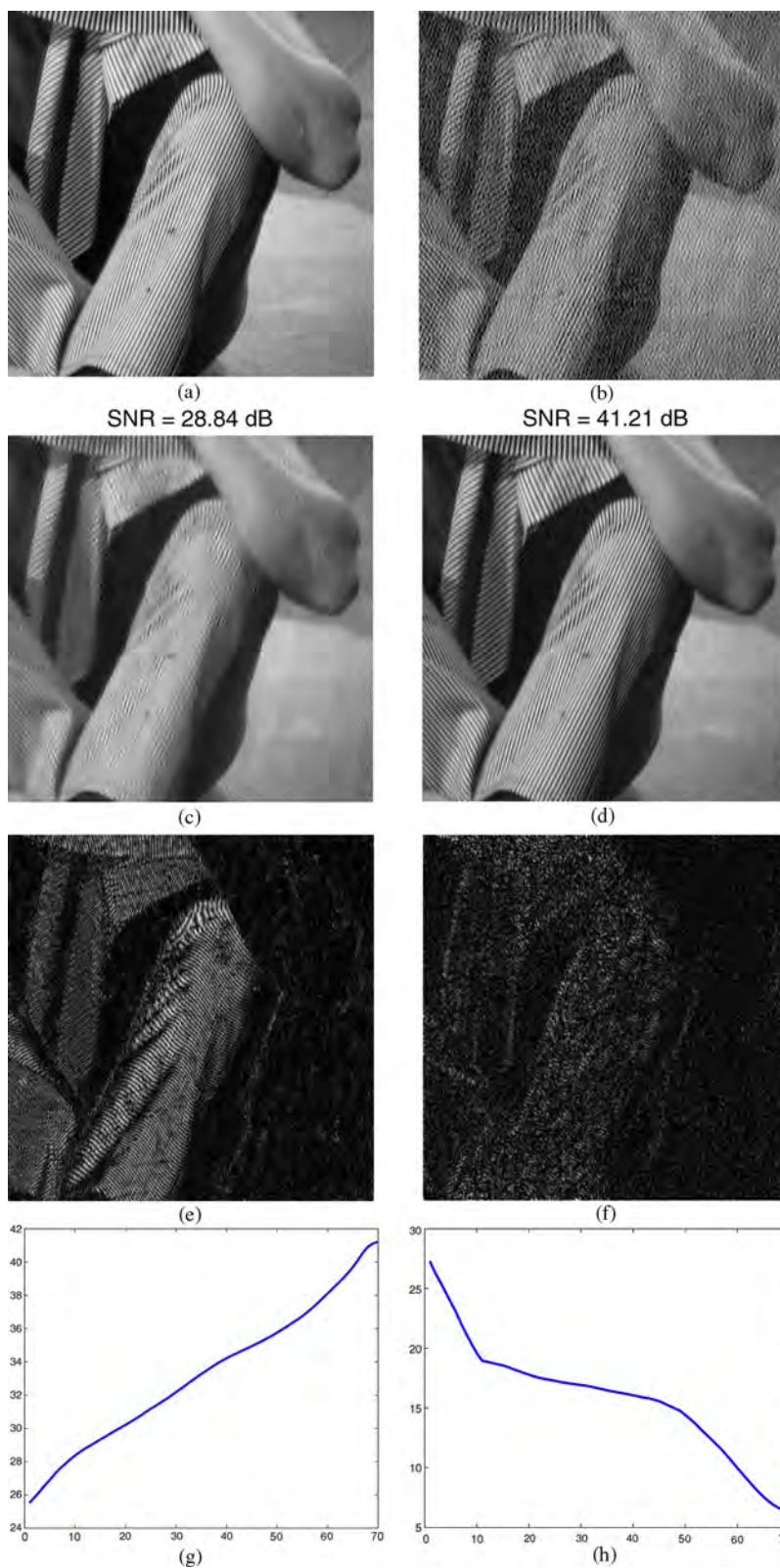


Fig. 6. Compressed measurement for a standard textural data. (a) Original data. (b) Zero-filling reconstruction. (c) *Wavelet-TV* recovery. (d) Recovery by the proposed method. (e) and (f) Removed components by (c) and (d). (g) and (h) SNR and recovery errors versus number of iterations. The horizontal coordinate in (g) and (h) denotes the number of iterations, and the vertical coordinate denotes SNR in (g) and recovery errors in (h).

curvelet partial reconstruction has better performance than wavelet reconstruction. Curvelet transform preserves the edges of scratches, while the wavelet transform results in oscillation artifacts along the edges. The good compressibility of surfaces

in the directional wavelet domain makes it possible to apply the CS for surface metrology.

In the first example, we apply the proposed compressed measurement method for a “Lena” image that is a standard

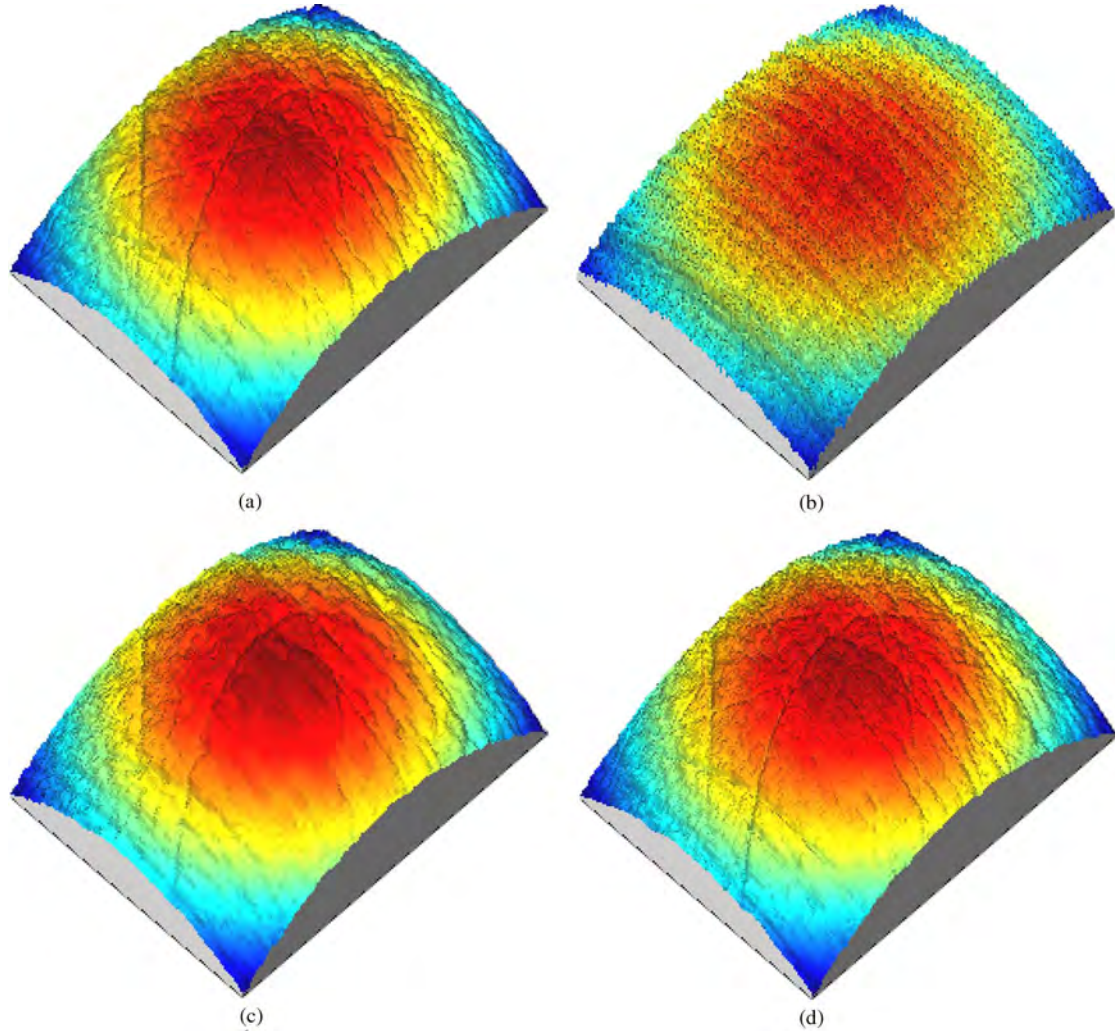


Fig. 7. Compressed measurement for a raw joint surface. (a) Original surface. (b) Zero-filling reconstruction. (c)  $l_1 - TV$  recovery. (d) recovery by the proposed method.

textural data. Fig. 6(a) shows the original data. We consider the 25% partial random measurement in the Fourier space [30]. The measurement sampling strategy will be emphasized at the end of this section. Fig. 6(b) is a zero-filling reconstruction from the incomplete  $K$ -space measurement. Fig. 6(c) is obtained using *wavelet-TV* recovery, i.e., solving minimization of  $\|\vartheta\|_{l_1} + TV(x)$ , subject to  $\|\hat{A}\vartheta - y\| \leq \epsilon$  by a nonlinear conjugate gradient method [30]. The signal-to-noise ratio (SNR) achieved is 28.84 dB. Fig. 6(d) is the recovery data using our iterative curvelet thresholding, where we take the zero-filling reconstruction as an initial data and use a linear decaying threshold value  $\sigma_0(1 - n/M)$ , in which  $M = 70$  is the total number of iterations,  $n$  is an index of iterations, and the initial threshold  $\sigma_0 = 0.05$ . The SNR of the recovered image is 41.21 dB. Fig. 6(e) shows the lost components (i.e., the difference between the recovery and original data) by the *wavelet-TV* method. Fig. 6(f) shows the lost components by the proposed method. It can clearly be seen that the proposed method recovers the edges and textures much better than other methods. Fig. 6(g) shows the changes in the SNR as the number of iterations increases, and Fig. 6(h) shows the changes of  $l_1$ -norm errors between the recovery

and original data (i.e.,  $\|x - x_0\|_{l_1}$ ) as the number of iterations increases.

After the encouraging results on modeling examples, we show the abilities of the proposed method to extract and recover scratches from microscaler surfaces of biomedical implanted joints. The metrology of the surfaces is related to biological compatibility and life expectancy of joints. Fig. 7(a) displays a raw surface topography from a worn metallic joint head with morphological structures consisting of roughness and deep scratches. The sampling interval in the horizontal  $x$ - and  $y$ -directions of the surface is 0.952 and 0.817  $\mu\text{m}$ , and that in the vertical direction is 1  $\mu\text{m}$ . The number of sampling points is  $240 \times 368$ . We again use the  $K$ -space random measurement matrix. Fig. 7(b) is the zero-filling reconstruction, and Fig. 7(c) is the  $l_1$ -TV reconstruction, i.e., solving the minimization of  $\|x\|_{l_1} + TV(x)$ , subject to  $\|\Phi x - y\| \leq \epsilon$  [6], [30]. Fig. 7(d) is the recovery by our iterative curvelet thresholding. Again, we show the performance of the proposed method for a surface measured from another worn femoral head of orthopedic implant shown in Fig. 8(a). Fig. 8(b)–(d) is obtained by zero-filling reconstruction,  $l_1$ -TV, and our iterative curvelet thresholding, respectively. Our method recovers the scratches very well. It

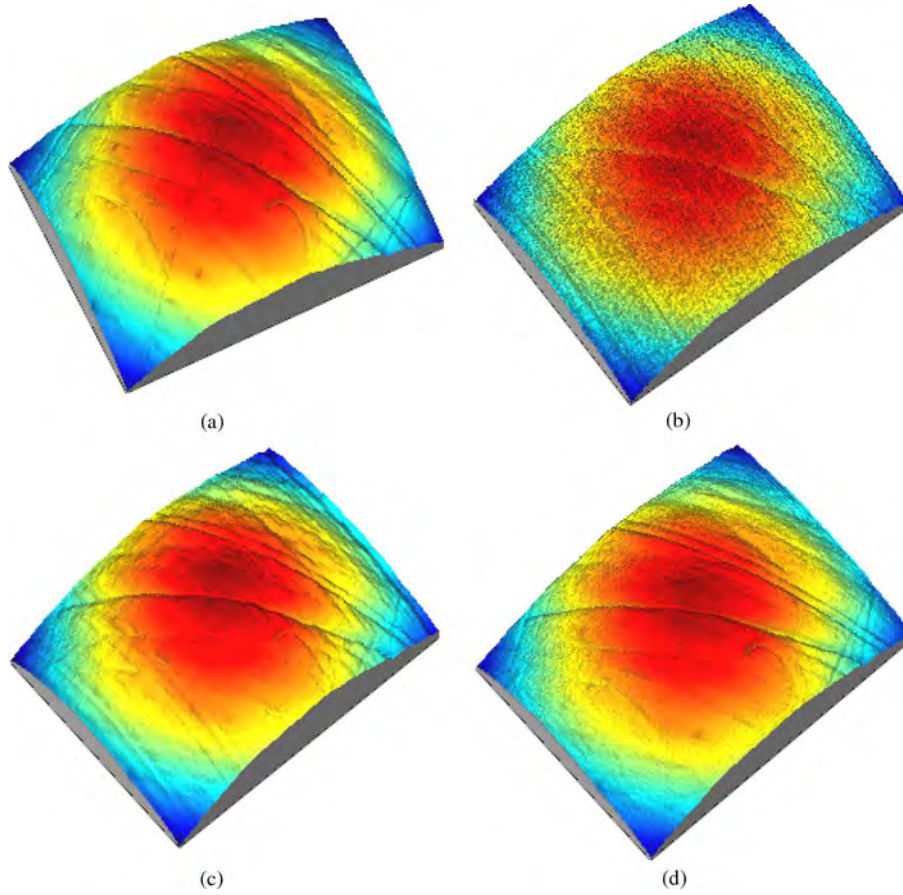


Fig. 8. (a) original surface. (b) zero-filling reconstruction. (c)  $l_1$ -TV recovery. (d) Recovery by the proposed method.

should be noted that a  $K$ -space measurement noise (produced by 0.05 times of random numbers) is considered in the two tests above.

Other engineering surfaces are also considered. Fig. 9(a) shows a honed surface of an automotive engine cylinder. The sampling interval in the horizontal  $x$ - and  $y$ -directions of the surface is 16 and 16  $\mu\text{m}$ , and that in the vertical direction is 5.3  $\mu\text{m}$ . The surface including the form, waviness, and roughness components that almost submerge the main features of the deep valleys or pits. Usually, the most important features that affect the performance of the cylinder are deep valleys whose distribution and amplitude will considerably influence the flow of gas or air in a pressure balance of an engine. Detection of these features is also useful for online manufacture monitoring. Fig. 9(b) and (c) is recovered by zero-filling reconstruction and iterative curvelet thresholding. We see that the proposed method can recover the surfaces almost exactly from the incomplete measurement. Fig. 9(d) is obtained to extract the deep valleys directly from compressed measurement for morphological assessment by the iterative curvelet thresholding using an experiential threshold value. Here, we want to show that it is also possible to directly extract scratched features (e.g., by using suitable thresholding) for metrology from the highly incomplete random measurements without the need to recover the full original surface first.

Now, we show the ability of the compressed measurement based on the wave atom transform. Fig. 10(a) shows a very

noise surface. We consider measurement noises at the same time. The sampling interval in the horizontal  $x$ - and  $y$ -directions of the surface is 6.6 and 7.7  $\mu\text{m}$ , and that in the vertical direction is 1.2  $\mu\text{m}$ . The number of sampling points is  $256 \times 256$ . Fig. 10(b) is the *wavelet-TV* recovery. Fig. 10(c) and (d) shows the surface with extracted scratches by curvelet thresholding with 30 iterations and wave atom thresholding with five iterations. Wave atoms are more sparse for such a textural surface. The proposed compressed measurement methods are robust for surfaces with noise and measurement errors.

Finally, it should be emphasized that random point undersampling with a factor of 0.25 (i.e., 25% measurements) from a Cartesian grid in Fourier measurement space has been applied in the above experiments. The Fourier measurements can easily be implemented by existing optical imaging instruments. Fig. 11 shows an example for the sampling pattern with its sampling probability density function. Various measurement numbers would result in different accuracy and convergence to some extent. Taking the honed surface (shown in Fig. 9) as an example, Fig. 12 shows the comparisons of SNR and  $l_1$ -norm recovery errors as the number of iterations increases by using undersampling measurement with a factor of 0.25 (shown as a real line) and with a factor of 0.1 (shown as a dashed line).

Furthermore, Fig. 13 is an example showing how the accuracy of the retrieved surface is influenced, depending on the number of samples, and showing when the proposed method fails. Fig. 13 shows the changes of SNR and recovery errors

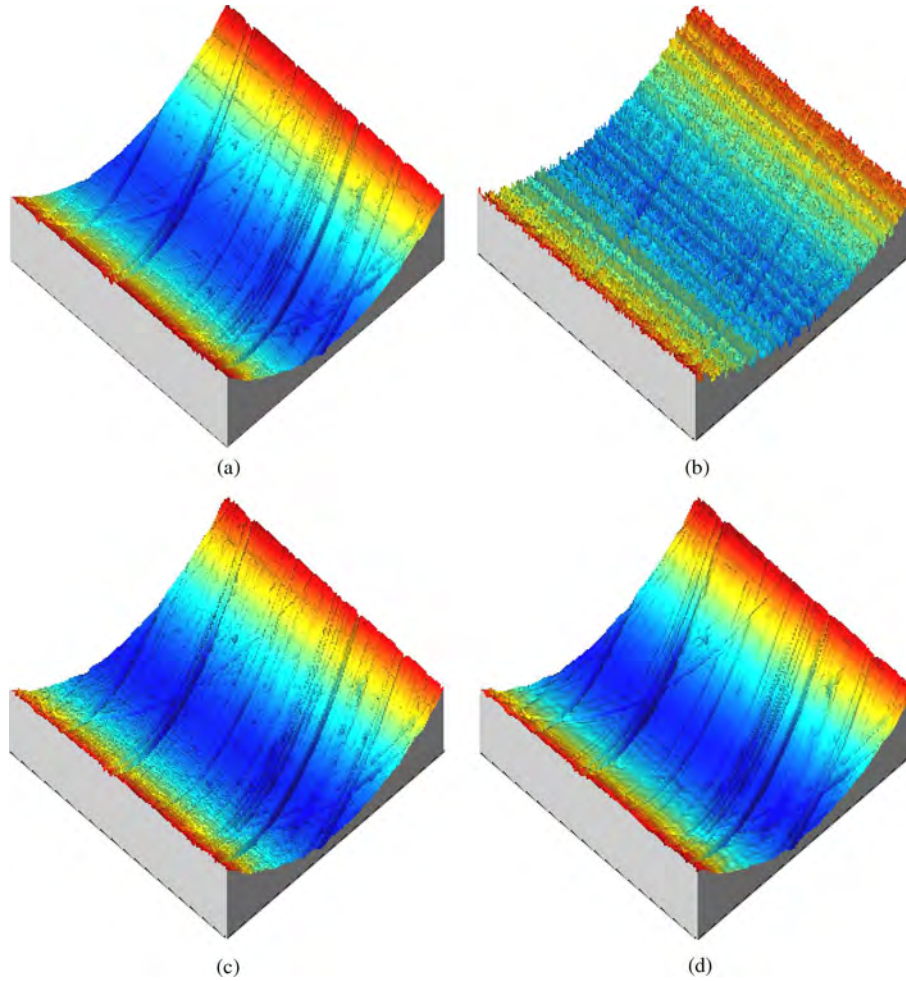


Fig. 9. Compressed measurement for a honed surface of the automotive engine cylinder. (a) Original surface. (b) Zero-filling reconstruction. (c) Iterative curvelet thresholding using linear decaying threshold values from the maximum value to zero. (d) Iterative curvelet thresholding using a suitable threshold values that does not tend to zero.

as the number of measurements increases from 10% samples to 55% samples. The upper row shows the results by using the iterative curvelet thresholding with 30 iterations and  $\sigma_0 = 0.06$ . It can be seen clearly that the minimum number of measurements for this case is 30% of the samples so as to obtain a satisfying recovery sequence. The lower row shows the results by using 50 iterations, where the case with 20% measurements is also a satisfying point. Results are mainly related to measurement matrices in the encoding step and parameters of the recovery algorithm in the decoding step. Because the random measurement strategy is used in our experiments, the measurement matrix is different for each implementation, which also leads to a slight different recovery to some extent. Normally, one can use less iterative times for a case with more measurements. Once a safe or quality-guaranteed number of measurements is used, the proposed method can balance the cost of encode and decode according to our practical requirements.

Other sampling trajectories, such as parallel-line, radial-line, or spiral sampling, can also be applied for the compressed measurement [31]. Furthermore, variable-density sampling can be used to match the nonuniform energy distribution of surfaces in the Fourier space. These complex sampling trajectories are irregular in a non-Cartesian grid, which involves nonequispaced

Fourier transform. The choice of trajectory is application dependent, where one has to consider surface characteristics and instrumental considerations. In practice, we can choose the sampling trajectories or measurement strategy obeying the following rule: 1) There should be lower coherence to sparse basis; 2) it should be easily implemented by measurement instruments; and 3) a fast nonlinear recovery algorithm can be applied for this sampling trajectory.

## VI. CONCLUSION

This paper has considered a problem of surface metrology with highly incomplete measurements. The novelty of this paper includes the following two aspects.

- 1) A compressed measurement mechanism for surface metrology was proposed, inspired by a new concept named compressive sampling from information theorem, which is used to solve undetermined ill-posed inverse problems. The compressed metrology enables us to accurately and robustly recover surfaces from an incomplete set of measurements dictated by geometric and structured features, rather than its Fourier bandwidth limited by the Shannon sampling theorem. In particular, one only needs

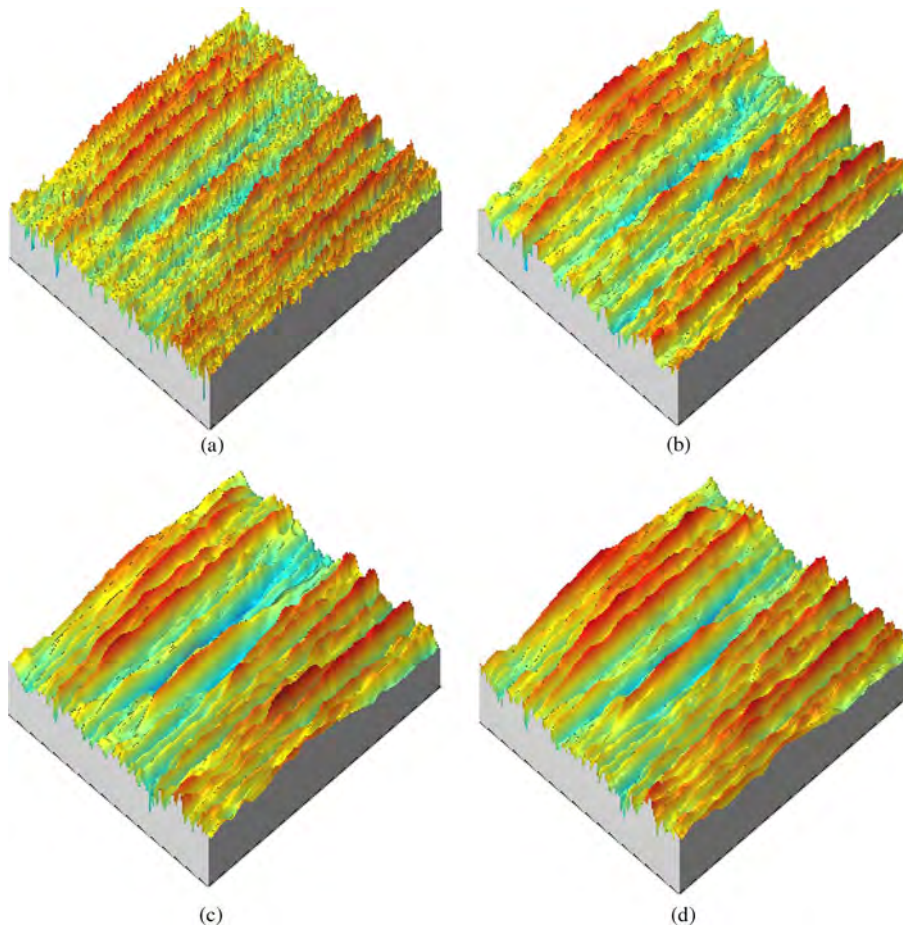


Fig. 10. Compressed metrology for a noise microscalar engineering surface. (a) Original surface. (b) *Wavelet-TV* recovery. (c) Iterative curvelet thresholding with 30 iterations. (d) Iterative wave atom thresholding with five iterations.

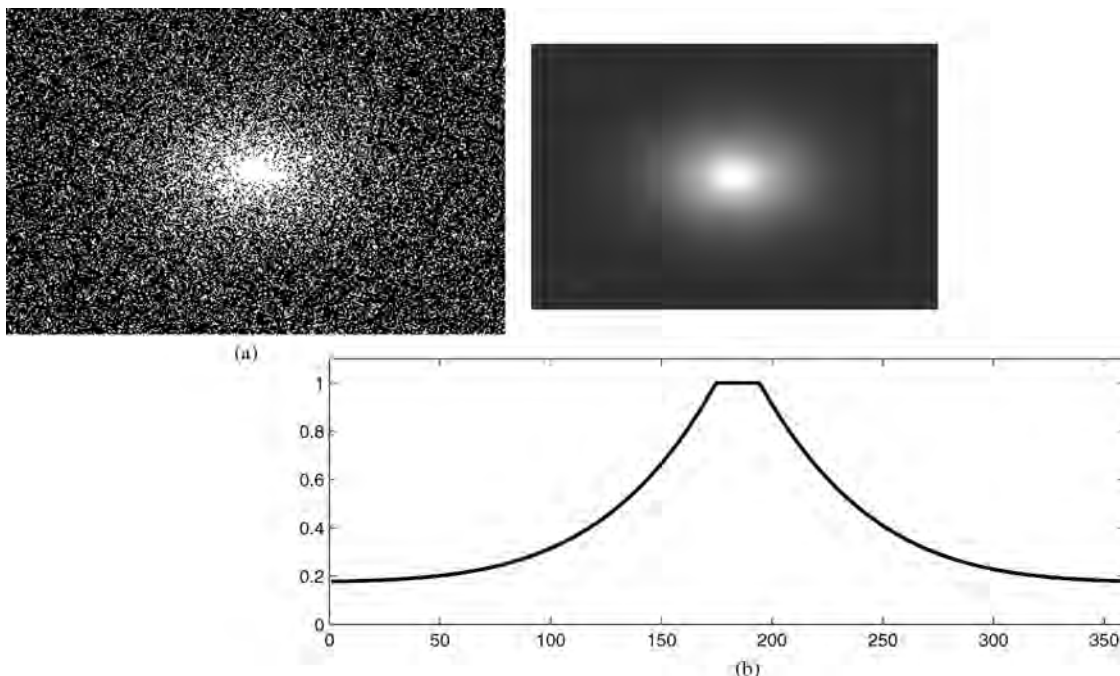


Fig. 11. Random point undersampling with a factor of 0.25 from a Cartesian grid in the Fourier measurement space. (a) Sampling pattern (the white points denotes sampling points). (b) Sampling probability density function (the upper subfigure is its 2-D density function and the lower subfigure is its 1-D center profile, and the horizontal coordinate denotes the sample).

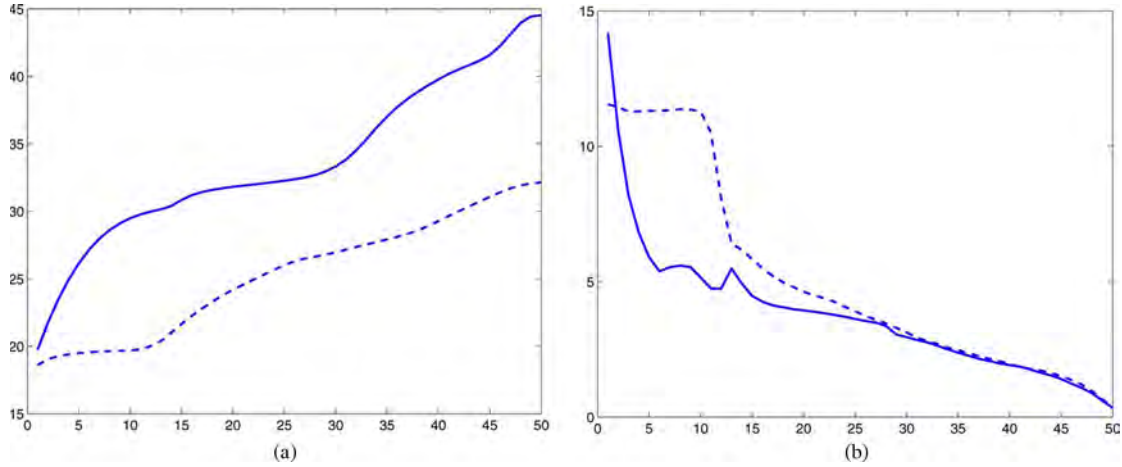


Fig. 12. Comparisons of (a) SNR and (b)  $l_1$ -norm errors as iterative number increases using different undersampling factors for the honed surface of an automotive engine cylinder. The real line denotes the case using 25% measurements, and the dashed line denotes 10% measurements. The horizontal coordinate denotes the number of iterations. The vertical coordinate denotes the value of SNR in (a) and recovery errors in (b).

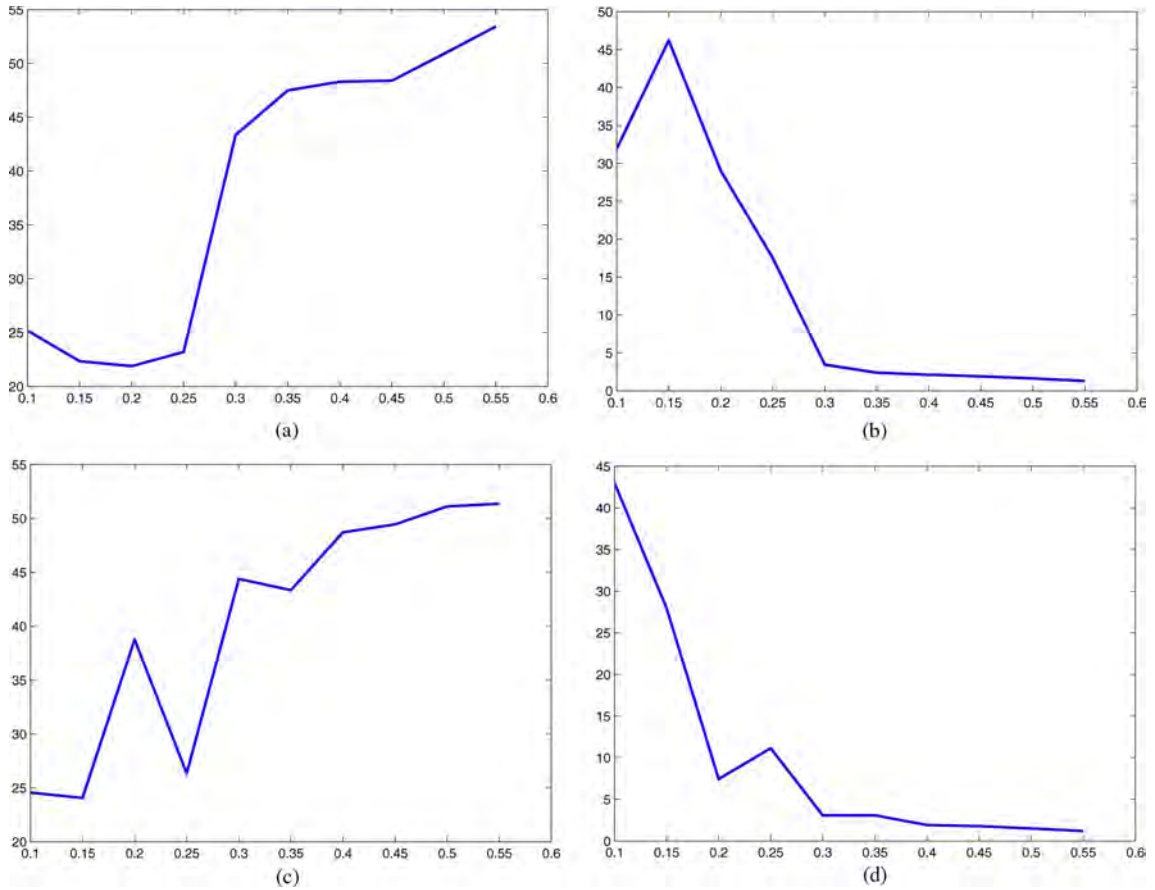


Fig. 13. (a) and (c) SNR versus number of measurements (or sampling points). (b) and (d) Recovery errors versus number of measurements. The horizontal coordinate denotes the ratio of number of measurements. The vertical coordinate denotes the value of SNR in (a) and (c) and recovery errors in (b) and (d). The iterative curvelet thresholding with 30 iterations has been used for recovery in the upper row and with 50 iterations in the lower row.

$O(S \cdot \log(N/S))$  random measurement to recover an  $S$ -sparse  $N \times N$  surface.

- 2) A convex-optimization solution with multiscale and multidirectional sparse constrains was provided for non-linear recovery of the compressed measurements using iterative curvelet/wave atom thresholding methods. The proposed methods are particularly suitable for surfaces with scratches and textures.

The CS makes us to rethink sensing mechanisms for surface metrology. If surfaces are compressible in an appropriate transform domain, we can design a sensing mechanism that are low incoherent to this transform to sparsely measure the surfaces. The technique can be applied to various instruments, such as the stylus, CT, and SEM, and would be significant for ongoing applications for precision engineering involving metrology, tribology, physics, and medical and biological engineering.

Finally, we present the following new directions and open problems for compressed measurements in future research.

- 1) How can we design an optimal sampling scheme with low-rate incoherent measurements for numerous real surfaces?
- 2) How can we design CS measurement devices (e.g., an optical imaging system) according the sampling scheme that directly records compressed patterns for practical applications?
- 3) Can we implement the wavelet transform or curvelet transform by an optical measurement system? Can we consider the sparse measurement in wavelet domain instead of Fourier domain?
- 4) How can we speed up the decoding recovery algorithm?
- 5) How can we estimate roughness parameters ( $R_a$ ,  $R_q$ ,  $R_v$ , etc.) directly from the compressed measurements while do not need to recover full surface first?

#### ACKNOWLEDGMENT

The author would like to thank the editors and referees for their constructive suggestions, which substantially improved this paper, L. Blunt, X. Jiang, and P. Scott of the Center for Precision Technology at the University of Huddersfield (U.K.) for the previous discussions on surface metrology, A. Antoniadis of the University of Joseph Fourier (France), and G. Plonka of the University of Duisburg-Essen (Germany) for the stimulating discussions on curvelets.

#### REFERENCES

- [1] A. Antoniadis and J. Fan, "Regularization of wavelet approximation," *J. Amer. Stat. Assoc.*, vol. 96, no. 455, pp. 939–967, Sep. 2001.
- [2] R. Baraniuk, "A lecture on compressive sensing," *IEEE Signal Process. Mag.*, vol. 24, no. 4, pp. 118–121, Jul. 2007.
- [3] T. Blumensath and M. E. Davies, "Iterative thresholding for sparse approximations," *J. Fourier Anal. Appl.*, vol. 14, no. 5/6, pp. 629–654, Dec. 2008.
- [4] C. Brown, W. Johnsen, and K. Hult, "Scale-sensitivity, fractal analysis and simulations," *Int. J. Mach. Tools Manuf.*, vol. 38, no. 5/6, pp. 633–637, May/Jun. 1998.
- [5] E. J. Candès and T. Tao, "Decoding by linear programming," *IEEE Trans. Inf. Theory*, vol. 51, no. 12, pp. 4203–4215, Dec. 2005.
- [6] E. J. Candès, J. Romberg, and T. Tao, "Stable signal recovery from incomplete and inaccurate information," *Commun. Pure Appl. Math.*, vol. 59, no. 8, pp. 1207–1233, Aug. 2006.
- [7] E. J. Candès and T. Tao, "Near optimal signal recovery from random projections: Universal encoding strategies," *IEEE Trans. Inf. Theory*, vol. 52, no. 12, pp. 5406–5425, Dec. 2006.
- [8] E. J. Candès, J. Romberg, and T. Tao, "Robust uncertainty principles: Exact signal reconstruction from highly incomplete frequency information," *IEEE Trans. Inf. Theory*, vol. 52, no. 2, pp. 489–509, Feb. 2006.
- [9] E. J. Candès, "Compressive sampling," in *Proc. Int. Congr. Mathematicians*, Madrid, Spain, 2006, vol. 3, pp. 1433–1452.
- [10] E. J. Candès and M. B. Wakin, "An introduction to compressive sampling," *IEEE Signal Process. Mag.*, vol. 25, no. 2, pp. 21–30, Mar. 2008.
- [11] E. J. Candès and D. L. Donoho, "New tight frames of curvelets and optimal representations of objects with piecewise  $C^2$  singularities," *Commun. Pure Appl. Math.*, vol. 57, no. 2, pp. 219–266, Feb. 2004.
- [12] E. J. Candès, L. Demanet, D. L. Donoho, and L. Ying, "Fast discrete curvelet transforms," *Multiscale Model. Simul.*, vol. 5, no. 3, pp. 861–899, Jan. 2006.
- [13] X. Chen, J. Raja, and S. Simanapalli, "Multi-scale analysis of engineering surfaces," *Int. J. Mach. Tools Manuf.*, vol. 35, no. 2, pp. 231–238, Feb. 1995.
- [14] I. Daubechies, *Ten Lectures on Wavelets*. Philadelphia, PA: SIAM, 1992.
- [15] I. Daubechies, M. De Fries, and C. De Mol, "An iterative thresholding algorithm for linear inverse problems with a sparsity constraint," *Commun. Pure Appl. Math.*, vol. 57, no. 11, pp. 1413–1457, Nov. 2004.
- [16] I. Daubechies, M. Fornasier, and I. Loris, "Accelerated projected gradient method for linear inverse problems with sparsity constraints," *J. Fourier Anal. Appl.*, vol. 14, no. 5/6, pp. 764–792, Dec. 2008.
- [17] L. Demanet and L. Ying, "Wave atoms and sparsity of oscillatory patterns," *Appl. Comput. Harmon. Anal.*, vol. 23, no. 3, pp. 368–387, Nov. 2007.
- [18] R. De Vore, "Deterministic constructions of compressed sensing matrices," *J. Complex.*, vol. 23, no. 4–6, pp. 918–925, Aug. 2007.
- [19] M. Do and M. Vetterli, "The contourlet transform: An efficient directional multiresolution image representation," *IEEE Trans. Image Process.*, vol. 14, no. 12, pp. 2091–2106, Dec. 2005.
- [20] D. Donoho, "Compressed sensing," *IEEE Trans. Inf. Theory*, vol. 52, no. 4, pp. 1289–1306, Apr. 2006.
- [21] M. Duarte, M. Davenport, D. Takhar, J. Laska, T. Sun, K. Kelly, and R. Baraniuk, "Single-pixel imaging via compressive sampling," *IEEE Signal Process. Mag.*, vol. 25, no. 2, pp. 83–91, Mar. 2008.
- [22] M. Elad, "Optimized projections for compressed sensing," *IEEE Trans. Signal Process.*, vol. 55, no. 12, pp. 5695–5702, Dec. 2007.
- [23] M. Elad, B. Matalon, J. Shtok, and M. Zibulevsky, "A wide-angle view at iterated shrinkage algorithms," in *Proc. SPIE—Wavelet XII*, San Diego, CA, Aug. 2007, vol. 6701, p. 670 102.
- [24] M. Figueiredo, R. Nowak, and S. Wright, "Gradient projection for sparse reconstruction: Application to compressed sensing and other inverse problems," *IEEE J. Sel. Topics Signal Process.*, vol. 1, no. 4, pp. 586–597, Dec. 2007.
- [25] M. Fornasier and H. Rauhut, "Iterative thresholding algorithms," *Appl. Comput. Harmon. Anal.*, vol. 25, no. 2, pp. 187–208, Sep. 2008.
- [26] G. Kaiser, *A Friendly Guide to Wavelets*. Boston, MA: Birkhauser, 1994.
- [27] P. Indyk, "Explicit constructions for compressed sensing of sparse signals," in *Proc. 19th Symp. Discr. Algorithms*, 2008, pp. 30–33.
- [28] X. Jiang, L. Blunt, and K. J. Stout, "Development of a lifting wavelet representation for surface characterization," *Proc. R. Soc. Lond. A, Math. Phys. Sci.*, vol. 456, no. 2001, pp. 2283–2313, Sep. 2000.
- [29] B. Josso, D. Burton, and M. Lalor, "Wavelet strategy for surface roughness analysis and characterization," *Comput. Methods Appl. Mech. Eng.*, vol. 191, no. 8–10, pp. 829–842, Dec. 2001.
- [30] M. Lustig, D. Donoho, and J. Pauly, "Sparse MRI: The application of compressed sensing for rapid MR imaging," *Magn. Reson. Med.*, vol. 58, no. 6, pp. 1182–1195, Dec. 2007.
- [31] M. Lustig, D. Donoho, J. Santos, and J. Pauly, "Compressed sensing MRI," *IEEE Signal Process. Mag.*, vol. 25, no. 2, pp. 72–82, Mar. 2008.
- [32] J. Ma, X. Jiang, and P. Scott, "Complex ridgelets for shift invariant characterization of surface topography with line singularities," *Phys. Lett. A*, vol. 344, no. 6, pp. 423–431, Sep. 2005.
- [33] J. Ma, "Towards artifact-free characterization of surface topography using complex wavelets and total variation minimization," *Appl. Math. Comput.*, vol. 170, no. 2, pp. 1014–1030, Nov. 2005.
- [34] J. Ma and M. Fenn, "Combined complex ridgelet shrinkage and total variation minimization," *SIAM J. Sci. Comput.*, vol. 28, no. 3, pp. 984–1000, 2006.
- [35] J. Ma, "Curvelets for surface characterization," *Appl. Phys. Lett.*, vol. 90, no. 5, p. 054 109, Jan. 2007.
- [36] J. Ma, "Characterization of textural surfaces using wave atoms," *Appl. Phys. Lett.*, vol. 90, no. 26, p. 264 101, Jun. 2007.
- [37] J. Ma, A. Antoniadis, and F.-X. Le Dimet, "Curvelet-based snake for multiscale detection and tracking of geophysical fluids," *IEEE Trans. Geosci. Remote Sens.*, vol. 44, no. 12, pp. 3626–3638, Dec. 2006.
- [38] J. Ma and G. Plonka, "Combined curvelet shrinkage and nonlinear anisotropic diffusion," *IEEE Trans. Image Process.*, vol. 16, no. 9, pp. 2198–2206, Sep. 2007.
- [39] J. Ma and G. Plonka, "A review of curvelets and recent applications," *IEEE Signal Process. Mag.*, 2009, to be published.
- [40] J. Ma and G. Plonka, "Computing with curvelets: From image processing to turbulent flows," *IEEE Comput. Sci. Eng.*, vol. 11, no. 2, pp. 72–80, Mar./Apr. 2009.
- [41] J. Ma and F.-X. Le Dimet, "Deblurring from highly incomplete measurements for remote sensing," *IEEE Trans. Geosci. Remote Sens.*, vol. 47, no. 3, pp. 792–802, Mar. 2009.
- [42] G. Peyré, "Best basis compressed sensing," in *Proc. SSVM*, Jun. 2007, pp. 80–91.
- [43] E. Le Pennec and S. Mallat, "Sparse geometrical image approximation with bandlets," *IEEE Trans. Image Process.*, vol. 14, no. 4, pp. 423–438, Apr. 2005.

- [44] J. Raja, B. Muralikrishnan, and S. Fu, "Recent advances in separation of roughness, waviness and form," *Precis. Eng.*, vol. 26, no. 2, pp. 222–235, Apr. 2002.
- [45] L. Rudin, S. Osher, and E. Fatemi, "Nonlinear total variation noise removal algorithm," *Phys. D*, vol. 60, no. 1–4, pp. 259–268, Nov. 1992.
- [46] R. Scott, P. Ungar, T. Bergstrom, C. Brown, F. Grine, M. Teaford, and A. Walker, "Dental microwear texture analysis shows within-species diet variability in fossil hominins," *Nature*, vol. 436, no. 7051, pp. 693–695, Aug. 2005.
- [47] J. L. Starck, E. J. Candès, and D. L. Donoho, "The curvelet transform for image denoising," *IEEE Trans. Image Process.*, vol. 11, no. 6, pp. 670–684, Jun. 2002.
- [48] J. A. Tropp and A. C. Gilbert, "Signal recovery from random measurements via orthogonal matching pursuit," *IEEE Trans. Inf. Theory*, vol. 53, no. 12, pp. 4655–4666, Dec. 2007.
- [49] L. Villemoes, "Wavelet packets with uniform time–frequency localization," *C. R. Acad. Sci. Paris*, vol. 335, no. 10, pp. 793–796, Nov. 2002.
- [50] D. J. Whitehouse, "Surface metrology," *Meas. Sci. Technol.*, vol. 8, no. 9, pp. 955–972, Sep. 1997.
- [51] J. Xu and S. Osher, "Iterative regularization and nonlinear inverse scale space applied to wavelet based denoising," *IEEE Trans. Image Process.*, vol. 16, no. 2, pp. 534–544, Feb. 2007.



**Jianwei Ma** received the Ph.D. degree in solid mechanics from Tsinghua University, Beijing, China, in 2002.

He has been a Visiting Scholar, Research Fellow, Postdoctoral Scientist, and Guest Professor with the University of Cambridge, Cambridge, U.K., the University of Oxford, Oxford, U.K., the University of Huddersfield, Huddersfield, U.K., the University of Mannheim, Mannheim, Germany, Institut National de Recherche en Informatique et Automatique (INRIA), Paris, France, and the University of Duisburg-Essen, Duisburg-Essen, Germany. Since 2006, he has been an Assistant Professor with the School of Aerospace, Tsinghua University. From June to August 2006, he was a Visiting Professor with the Swiss Federal Institute of Technology (EPFL), Lausanne, Switzerland. From June to September 2007, he was a Visiting Professor with Florida State University, Tallahassee, FL, and the University of Colorado, Boulder. In May 2008, and from March to September 2009, he was an Invited Professor with INRIA-Grenoble and Ecole des Mines de Paris, Fontainebleau, France. He is an Editor of the *International Journal of Artificial Intelligence*. He is the author or a coauthor of about 40 papers in refereed journals. His research interests include wavelets, curvelets, image processing, compressed sensing, surface metrology, aerospace remote sensing, and seismic exploration.

# Compressed Sensing for Surface Characterization and Metrology

Jianwei Ma

**Abstract**—Surface metrology is the science of measuring small-scale features on surfaces. In this paper, a novel compressed sensing (CS) theory is introduced for the surface metrology to reduce data acquisition. We first describe that the CS is naturally fit to surface measurement and analysis. Then, a geometric-wavelet-based recovery algorithm is proposed for scratched and textural surfaces by solving a convex optimal problem with sparse constrained by curvelet transform and wave atom transform. In the framework of compressed measurement, one can stably recover compressible surfaces from incomplete and inaccurate random measurements by using the recovery algorithm. The necessary number of measurements is far fewer than those required by traditional methods that have to obey the Shannon sampling theorem. The compressed metrology essentially shifts online measurement cost to computational cost of offline nonlinear recovery. By combining the idea of sampling, sparsity, and compression, the proposed method indicates a new acquisition protocol and leads to building new measurement instruments. It is very significant for measurements limited by physical constraints, or is extremely expensive. Experiments on engineering and bioengineering surfaces demonstrate good performances of the proposed method.

**Index Terms**—Compressed sensing (CS)/compressive sampling, curvelets, incomplete measurement, sparse recovery, surface characterization, surface metrology, wave atoms.

## I. INTRODUCTION

**E**NGINEERING surfaces are composed of multiscale topographies, e.g., roughness, waviness, form errors, random ridges/valleys, and peaks/pits. The functional topographical features impact directly on the mechanical and physical properties of the whole system, such as wear, friction, lubrication, corrosion, fatigue, coating, and paintability in many disciplines, including tribology, fluid mechanics, optics, semiconductors, microelectronics, manufacturing, biology, and medicine. For instance, during the functional operation of interacting surfaces, peaks and ridges act as sites of high contact stress and abrasion, whereas the pits, valleys, and scratches (i.e., polish line or line-like wear) affect the lubrication and fluid retention properties. Surfaces also play a vital role in biology and medicine with most biological reactions occurring

Manuscript received March 5, 2008; revised May 4, 2009. This work was supported by the National Natural Science Foundation of China under Contract 40704019 and the Tsinghua Basic Research Fund under Contract JC2007030. The Associate Editor coordinating the review process for this paper was Dr. Emil Petriu.

The author is with the School of Aerospace, Tsinghua University, Beijing 100084, China, and also with the Centre de Geosciences, Ecole des Mines de Paris, 77305 Fontainebleau, France (e-mail: jma@tsinghua.edu.cn).

Color versions of one or more of the figures in this paper are available online at <http://ieeexplore.ieee.org>.

Digital Object Identifier 10.1109/TIM.2009.2027744

on surfaces and interfaces, *in vivo*. Surface metrology has also been used to support scientific discoveries in a variety of fields, including anthropology, archeology, geology, and biochemistry. Therefore, a highly accurate measurement, characterization, and metrology is an important issue for corresponding functional analysis [28], [29], [32], [33], [50].

Multiple methods were implemented to measure different characteristics, including engineering surfaces [50]. Methods including scan, ultrasonics, and scatter have also been developed. For instance, the metrological freak diffractometer based on the scattering method images the source in the Fourier transform plane: speckle techniques and holographic techniques for roughness measurement. Recent instruments including scanning electron microscope (SEM), scanning tunneling microscope, atomic force microscope, magnetic force microscopy, computer tomography (CT), and magnetic resonance imaging (MRI) have largely improved part of restrictions of conventional methods for different physical and medical applications. The versatility of instruments has allowed many different surface experiments to be carried out. These include the measurement and detection of growth in biological specimens, the initiation of some chemical reactions, the machining of substrates, and the microfabrication and movement of material around the surface.

All the aforementioned methods fall into direct measuring (e.g., stylus methods measure the roughness in space domain) and indirect measuring (e.g., CT and MRI collect data in the radon and Fourier transform domains, respectively). We propose here another approach named compressed measurement.

The traditional strategy of surface characterization (denoising, compression, feature extraction, etc.) and metrology requires exact measurements of full surface, computation of the complete set of filtering coefficients, selection of the significant coefficients, and reconstruction of these coefficients to get a required surface [28], [29], [32], [33]. Most existing methods for surface characterization and metrology follow this rule. However, very often, the number of measuring sensors may be limited by physical constraints, the measurements may be extremely expensive, or the sensing process may be slow so that one can only measure the object for a few times. The traditional strategy is extremely wasteful of the massive data acquisition and measuring time. Therefore, many researchers are seeking for methods of how one can reduce the amount of acquired data without degrading the metrology quality.

A novel theory named compressed sensing (CS) or compressive sampling has been proposed by Candès *et al.* [5]–[8] and Donoho [20] to answer the question of data acquisition. The basic principle of CS is that sparse or compressible

signals can be reconstructed from a surprisingly small set of measurements. Different from the classical Shannon sampling theorem or Nyquist rate, the sampling rate must be at least twice the maximum frequency presented in the signals; the CS says that one can recover certain signals from far fewer measurements than traditional methods use if the signals themselves are compressible. The term ‘‘compressible’’ means that the signals are sparse or transformed sparse, i.e., there are only very limited pixels or transformed coefficients with nonzero values. Actually, most natural and real-life surfaces are compressible in some fixed transforms such as discrete cosine transform, wavelet transform [14], [26], curvelet transform [11], [12], and wave atom transform [17]. A few potential applications of the CS theorem have been made in compressive imaging, wireless sensing networks, analog-to-information conversion, biosensing for deoxyribonucleic acid microarrays, etc. For details, we refer readers to several review papers [2], [9], [10].

Roughly speaking, if surfaces exhibit transform sparsity, and if incomplete measurements result in incoherent artifacts in the transform domain, then the surfaces can be recovered from the incomplete measurement by appropriate nonlinear recovery methods. In particular, if one measures linear combinations of Fourier coefficients (called  $K$ -space measurement blow), CS claims that the real surfaces can be accurately reconstructed from a small measured subset of  $K$ -space, rather than an entire  $K$ -space. In this paper, based on directional wavelet frames, we apply the idea of CS to surface metrology, renamed compressed measurement or compressed metrology, which directly concerns geometric and structural features instead of pixel’s information of surfaces.

The CS theory requires the following three aspects.

- 1) The desired surfaces are compressible, i.e., they have sparse representation in a known transform domain. In fact, real surfaces are naturally compressible in an appropriate transform. Here, we mainly care about the surfaces with scratches that are sparse in the curvelet transform domain and the surfaces with textures that are sparse in the wave atom domain.
- 2) The measurement matrices should be noise-like incoherent/uncorrelative to the sparse transforms. Normally, the measurement matrices can be taken as random matrices that are incoherent to almost all sparse transforms. CS combines the idea of sampling and compression, which can lead to build simpler and cheaper measurement instruments for metrology in many fields. How the measuring matrices are designed would indicate a design of new measurement instruments.
- 3) A nonlinear CS recovery algorithm, particularly an iterative curvelet/wave atom thresholding, is applied by solving a convex-optimization problem with sparse constrains.

It should be emphasized that the theme in this paper is totally different from our previous work in [32], [33], [35], and [36]. In previous work, we focus on surface sparse representation and feature extraction using sparse transforms. In this paper, we focus on imaging or measurement mechanism by apply-

ing a new mathematical theory named CS. The compressed-sensing measurement includes the following two steps: 1) on-line encoding measurement and 2) offline decoding recovery. In the offline recovery step, we also need to use some sparse transforms to build a sparse-promoting nonlinear recovery algorithm. In this paper, the sparse transforms are hired by an iterative thresholding framework for compressed-sensing recovery, instead of feature extraction. The sparse representation by curvelets and wave atoms addressed in previous papers [35], [36] can be seen as prior knowledge in the compressed-sensing measurement.

In the remainder of this paper, we first introduce the CS theory from the point of view of mathematics in Section II. In Section III, we describe that the curvelet transform and wave atom transform naturally fit for sparse representation of textural surfaces. Surfaces can be recovered stably by the proposed iterative curvelet and wave atom thresholding described in Section IV. Experiments on the compressed measurement for various surfaces are given in Section V. Finally, conclusions and a few new directions are drawn in Section VI.

## II. ENCODE: COMPRESSED MEASUREMENT

CS handles a fundamental problem of recovering a finite signal  $x$  from a limited set of random measurements  $y$ . This theory indicates that one can only do part of random measurements of engineering surfaces, instead of high-density measurements limited by the Shannon sampling theorem, to carry out highly accurate metrology. Let  $\Phi \in \mathcal{C}^{K,N}$ ,  $K \ll N$  be a so-called CS measurement matrix. Typical examples of the measurement matrices are Fourier transform  $F$  followed by a random undersampling operator  $R$ . The problem can be described as [6], [8]

$$y = \Phi x + \epsilon = R F x + \epsilon. \quad (1)$$

Here,  $\epsilon$  denotes the possible measurement errors or noise. Most of the time,  $x$  is not sparse in the space domain but is sparse in the transform domain by a basis  $\Psi$  (i.e.,  $x$  is transform sparse or compressible if the most coefficients concentrate near zeros). In this case, one can write (1) as

$$y = \Phi \Psi \vartheta + \epsilon. \quad (2)$$

To recover the sparse coefficient  $\vartheta$ , one solves an optimization problem by constructing the following cost function to be minimized:

$$\min_{\vartheta} \left\{ \|y - \tilde{A} \vartheta\|^2 + \lambda \sum_i^N p(|\vartheta_i|) \right\}, \quad \tilde{A} = \Phi \Psi. \quad (3)$$

Here, the first term denotes preserving information by measuring how close the decoding solution is to the input information. The second term is a regularization that represents *a priori* sparse information of original signals. The  $p$  is a function of  $\vartheta$ , and  $\lambda$  is a positive constant that determines the importance of the regularization term. This problem can also be solved

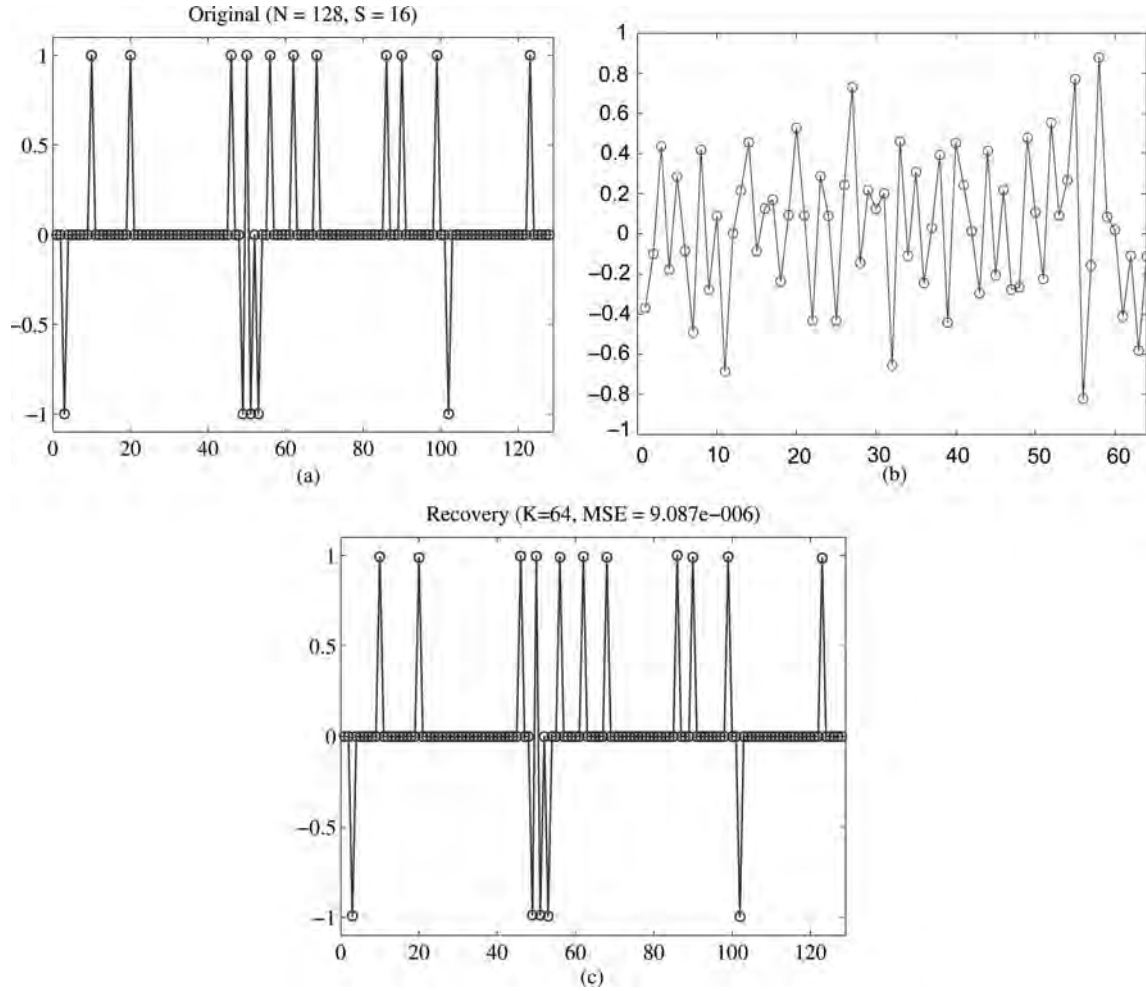


Fig. 1. One-dimensional sample for compressed sensing. (a) Original unknown signal. (b) Randomly measured signal. (c) Recovered signal by compressed sensing. The horizontal coordinate denotes sampling point, and the vertical coordinate denotes amplitude of the signal.

by  $l_1$ -minimization, which is also known as basis pursuit with inequality constraints and is described by [6]

$$\min_{\vartheta} \|\vartheta\|_{l_1}, \quad \text{subject to } \|\tilde{A}\vartheta - y\|_{l_2} \leq \epsilon. \quad (4)$$

If without considering the noise  $\epsilon$ , the convex optimization problem is a linear programming known as basis pursuit [5], which is given by

$$\min_{\vartheta} \|\vartheta\|_{l_1}, \quad \text{subject to } \tilde{A}\vartheta = y. \quad (5)$$

It seems hopeless to solving the underdetermined equations since the rows are much fewer than the columns in  $\tilde{A}$ . However, the CS has told us that if the signal  $x$  is sparse or compressible, the underdetermined system of equations can be exactly solved. Supposing that there are  $S$  nonzero coefficients (i.e., so-called  $S$ -sparse,  $\|\vartheta\|_{l_0} = S \ll N$ ), one just needs measurement numbers  $K$  in Fourier space with frequencies selected randomly, satisfying

$$K \geq C \cdot S \cdot \log N. \quad (6)$$

Let us first look at a 1-D example to understand the idea of CS. Assume that one has an unknown signal with  $N = 128$  sampling points and  $S = 16$  nonzero values, as shown in

Fig. 1(a). The numbers, positions, and values of the nonzero values are unknown in our experiment. One cannot use such information but can discover this information by the example algorithm. The *a priori* knowledge used is that the signal is sparse in the space domain. For instance, one considers a  $64 \times 128$  measurement matrix  $\Phi$  (i.e.,  $K = 64$ ) assembled by random numbers to measure the 1-D original unknown signal shown in Fig. 1(a). Each measurement, mathematically speaking, equals to an inner product of a row of the measurement matrix and the unknown signal. The measurements can be repeated up to 64 times using the different rows of the measurement matrix. Fig. 1(b) shows the measurement results. The CS says that one can exactly recover the unknown signal from these randomly measurements using nonlinear recovery methods. Fig. 1(c) displays a recovered signal from the incomplete measurements by using a so-called gradient projection for sparse reconstruction (GPSR) method proposed in [24]. The recovered signal is almost the same as original signal (the mean-square error  $\text{MSE} = 9.087e - 006$ ). Of course, for most applications, the usable *a priori* knowledge is the sparsity of signals in the transform domain instead of in the space domain. The surfaces that we handle in this paper are sparse in the curvelet and wave atom domains.

Naturally, the following two basic questions arise: 1) What are good CS matrices and how many measurements are required for successful reconstruction and 2) what are the most efficient decoder or recovery algorithm to solve the optimal problem?

To answer the first question, Candès *et al.* [5], [6] proposed a sufficient condition named restricted isometry property (RIP) for CS matrices. A measurement matrix  $\Phi$  satisfies the RIP of order  $S$  with constant  $\delta_S \in (0, 1)$ , if

$$(1 - \delta_S)\|x\|_{l_2}^2 \leq \|\Phi_T x\|_{l_2}^2 \leq (1 + \delta_S)\|x\|_{l_2}^2, \\ x \in R^N; \quad \|T\| \leq S. \quad (7)$$

Here,  $\Phi_T$ ,  $T \subset 1, \dots, N$ , denotes the  $K \times |T|$  submatrix obtained by extracting the columns of  $\Phi$  corresponding to the indices in  $T$ . The RIP says that the mapping  $\Phi$  acts like an isometry on  $S$ -space vectors. It requires that every set of columns with cardinality less than  $S$  approximately behaves like an orthonormal system. A measurement matrix  $\Phi$  satisfying the RIP ensures the exact and unique recovery to be obtained.

Furthermore, for compressible signals, a good measurement matrix should also be incoherent in the sparse basis. The greater incoherence of the measurement/sparsity pair  $(\Phi, \Psi)$  there is, the smaller the number of measurements will be needed. Supposing that  $\Phi$  is obtained by selecting  $K$  rows uniformly at random from an  $N \times N$  orthonormal matrix and renormalizing the columns so that they are unit normed, one has

$$S \leq C \cdot \frac{1}{v^2} \cdot \frac{K}{(\log N)^4} \quad (8)$$

where  $v := \sqrt{N} \max_{1 \leq i, j \leq N} |\langle \phi_i, \varphi_j \rangle|$  ( $\phi_i \in \Phi$ ,  $\varphi_j \in \Psi$ ) is referred to as the mutual coherent between the measurement basis  $\Phi$  and the sparsity basis  $\Psi$ . Generally,  $v(\Phi, \Psi) \in [1, \sqrt{N}]$ . In particular,  $v = 1$  when  $\Phi$  is the canonical or spike basis  $\phi_m(t) = \delta(t - m)$  and  $\Psi$  is the Fourier basis  $\varphi_j = N^{-1/2} e^{i2\pi jt/N}$ . That is to say, if  $\Phi$  is a partial Fourier matrix obtained by selecting  $K$  rows uniformly at random, we have  $S \leq C \cdot K/(\log N)^4$ . It has been known that noiselet measurement  $\Phi$  and Haar wavelets  $\Psi$  have mutual coherent  $v = \sqrt{2}$ ; noiselet measurement and Daubechies DB4 wavelets have  $v = \sqrt{2.2}$  [9]. Normally, one can choose random measurement matrices, which are largely incoherent to any fixed basis  $\Psi$ . The known CS measurement matrices  $\Phi$  satisfying the RIP are random matrices, including Gaussian, Bernoulli, and random partial bounded orthogonal matrices. Recently, how a deterministic and explicit measurement matrix is constructed has been concerned by De Vore [18] and Indyk [27]. How the design of the measurement matrices that need fewer measurement is optimized was also emphasized by Elad [22].

Assuming that the measurement matrix  $\Phi$  is an identity matrix  $I$  (i.e., without undersampling) and  $\Psi$  is a wavelet transform, the problem in (3) degenerates to the well-known wavelet regularization (see, e.g., [1]). This regularization is closely related to wavelet thresholding. Specifically, if the penalty function is taken as  $l_1$  penalty  $p(|\vartheta|) = |\vartheta|$ , the solution is a wavelet soft-thresholding rule; if the penalty function is given by  $p_\lambda(|\vartheta|) = \lambda^2 - (|\vartheta| - \lambda)^2 I(|\vartheta| < \lambda)$ , the solution is a hard-thresholding rule.

In addition to satisfying the RIP condition, the choice of  $\Phi$  depends on the physics of measurement problem. For example, in the case of scattered field, the electric field integral equations (operator  $\Phi$ ) are used for recovering the scatter geometry (signal  $x$ ) from the randomly incomplete measured scattered field (signal  $y$ ). In this paper, we consider an optical measurement system for frequency  $K$ -space measurements. The prior knowledge that we used in the framework of compressed measurement is that most scratched and textural surfaces can be sparsely represented by a  $\Psi$  called curvelet or wave atom transform. We proposed an iterative curvelet or wave atom thresholding as a nonlinear recovery algorithm for the compressed measurements. Now, the measurement matrix  $\Phi$  is a random sampling of Fourier coefficients of engineering surfaces, and original unknown surfaces or features  $x$  can be recovered from the measurements  $y$  by using the offline iterative thresholding methods. It is also possible to directly reconstruct the wanted features for metrology without the need to recover the full surface. The compressed measurement is a simple and efficient signal acquisition protocol with samples at a low rate and later uses computational power for optimal reconstruction from the incomplete set of measurements. The compressed measurement essentially shifts online measuring cost into offline computational cost of nonlinear recovery. Therefore, this metrology strategy can be called as computational metrology. Many existing sparse transforms and nonlinear optimal algorithms can be incorporated into the compressed measurement for various engineering surfaces.

### III. SPARSITY IN CURVELET AND WAVE ATOM DOMAINS

Sparse transforms have successfully been applied for surface metrology. An early method to be used as a filter is a Gaussian or spline filter. Although it has been widely used in surface metrology, the technique is insufficient in addressing the non-stationary and multiscale nature of rough surfaces. Applications of wavelets on surfaces analysis have become an increasing interest (see, e.g., [13], [28], [29], and [44] among a vast amount of current literature). The main advantages of wavelet-based methods are space–frequency localization and multiscale view of the features of surfaces. Unfortunately, traditional wavelets are not optimal to analyze surfaces with scratches or textures because wavelets ignore geometric properties of edges and textures, which leads to strong oscillating artifacts along the scratches of roughness (see [32]). Recently, Ma *et al.* [32]–[36] proposed a series of so-called artifact-free characteristic methods based on geometric wavelets. In particular, ridgelets, curvelets, and wave atoms have been applied to extract straight scratches, curve scratches, and textures from surfaces, respectively. It should also be noted that from another way, Brown *et al.* [4] considers the multiscale metrology by using a so-called scale-sensitive fractal analysis, which was recently used to characterize dental microwear textures in fossil hominid to understand the diets and evolution of our lineages [46]. However, the use of sparsity in inverse problems on data recovery is the most recent step.

Following the previous work on sparse representation of surfaces based on curvelets and wave atoms, we extend these

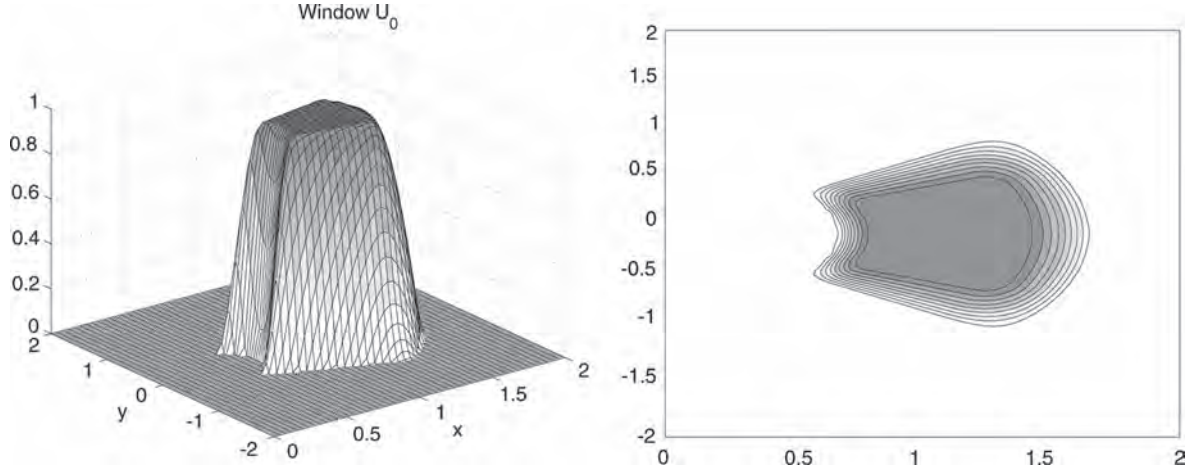


Fig. 2. (left) Window  $U_0(\xi)$ . (right) Its support.

sparse transforms to compressed measurement, which is a special inverse problem on recovery of incomplete data.

### A. Curvelets for Surfaces With Scratches

Curvelet transform allows an optimal sparse representation of objects with  $C^2$  singularities. The needle-shape elements of this transform own very high directional sensitivity and anisotropy. For a smooth object  $f$  with discontinuities along smooth curves, the best  $m$ -term approximation  $\tilde{f}_m$  by curvelet thresholding obeys  $\|f - \tilde{f}_m\|_2^2 \leq Cm^{-2}(\log m)^3$ , while for wavelets, the decay rate is only  $m^{-1}$ . Surprising performance has been shown in the fields of image processing, see, e.g., [35], [37], [38], [47]. It essentially obeys a parabolic scaling law between the width and length of an element (width  $\approx$  length<sup>2</sup>) and directional sensitivity (orientations =  $1/\sqrt{\text{scale}}$ ). See Fig. 1 (left) for an example of curvelet elements. Thus, it is good to characterize surfaces with general scratches. Several curvelet-like geometric multiscale transform, e.g., bandlets [43] and contourlets [19], have also been proposed to restore the curve singularities in a different way.

In the following, we give an outline for the second-generation discrete curvelet transform (DCuT) [11], [12], which is considerably simpler to use than the original first-generation formulation based on the block ridgelet transform. The second-generation DCuT is implemented by means of special frequency-window partitions. For details on curvelets, we refer to recent review papers [39], [40].

Let  $V(t)$  and  $W(r)$  be a pair of smooth nonnegative real-valued window functions such that  $V$  is supported on  $[-1, 1]$  and  $W$  on  $[1/2, 2]$ . The windows satisfy the admissibility conditions  $\sum_{l=-\infty}^{\infty} V^2(t-l) = 1$ ,  $t \in \mathbb{R}$ ,  $\sum_{j=-\infty}^{\infty} W^2(2^{-j}r) = 1$ ,  $r > 0$ . These conditions are satisfied, taking, e.g., the scaled Meyer windows [38], i.e.,

$$V(t) = \begin{cases} 1, & |t| \leq 1/3 \\ \cos \left[ \frac{\pi}{2} \nu(3|t| - 1) \right], & 1/3 \leq |t| \leq 2/3 \\ 0, & \text{else} \end{cases}$$

$$W(r) = \begin{cases} 1, & 5/6 \leq r \leq 4/3 \\ \cos \left[ \frac{\pi}{2} \nu(5 - 6r) \right], & 2/3 \leq r \leq 5/6 \\ \cos \left[ \frac{\pi}{2} \nu(3r - 4) \right], & 4/3 \leq r \leq 5/3 \\ 0, & \text{else} \end{cases}$$

where  $\nu$  is a smooth function satisfying

$$\nu(x) = \begin{cases} 0, & x \leq 0 \\ 1, & x \geq 1 \end{cases}, \quad \nu(x) + \nu(1-x) = 1; \quad x \in \mathbb{R}.$$

Let the Fourier transform of  $f \in L^2(\mathbb{R}^2)$  be defined by  $\hat{f}(\xi) := (1/2\pi) \int_{\mathbb{R}^2} f(x) e^{-i(x,\xi)} dx$ . Now, for  $j \geq 0$ , let the window  $U_j(\xi)$ ,  $\xi = (\xi_1, \xi_2) \in \mathbb{R}^2$  in the frequency domain be given by

$$U_j(\xi) = 2^{-3j/4} W(2^{-j}|\xi|) V(2^{\lfloor j/2 \rfloor} \theta), \quad \xi \in \mathbb{R}^2$$

where  $(|\xi|, \theta)$  denotes the polar coordinates corresponding to  $\xi$ . The support of  $U_j$  is a polar wedge determined by  $\text{supp } W(2^{-j}\cdot) = [2^{j-1}, 2^{j+1}]$  and  $\text{supp } V(2^{\lfloor j/2 \rfloor}\cdot) = [-2^{-\lfloor j/2 \rfloor}, 2^{-\lfloor j/2 \rfloor}]$ . Fig. 2 shows an example of the window  $U_0$  and its support [38].

The system of curvelets is now indexed by the following three parameters: 1) a scale  $2^{-j}$ ,  $j \in \mathbb{N}_0$ ; 2) an equispaced sequence of rotation angles  $\theta_{j,l} = 2\pi l \cdot 2^{-\lfloor j/2 \rfloor}$ ,  $0 \leq l \leq 2^{\lfloor j/2 \rfloor} - 1$ ; and 3) a position  $x_k^{(j,l)} = R_{\theta_{j,l}}^{-1}(k_1 2^{-j}, k_2 2^{-\lfloor j/2 \rfloor})^T$ ,  $(k_1, k_2) \in \mathbb{Z}^2$ , where  $R_{\theta_{j,l}}$  denotes the rotation matrix with angle  $\theta_{j,l}$ . The curvelets are defined by

$$\varphi_{j,l,k}(x) := \varphi_j \left( R_{\theta_{j,l}} \left( x - x_k^{(j,l)} \right) \right), \quad x = (x_1, x_2) \in \mathbb{R}^2$$

where  $\hat{\varphi}_j(\xi) := U_j(\xi)$ , i.e.,  $U_j$  is the Fourier transform of  $\varphi_j$ . Observe that in the spatial domain,  $\varphi_{j,l,k}$  rapidly decays outside of a  $2^{-j}$  by  $2^{-j/2}$  rectangle with center  $x_k^{(j,l)}$  and orientation  $\theta_{j,l}$  with respect to the vertical axis (see Fig. 3). Fig. 4 shows the support of windows at different scales and orientations. The wedges are longer and thinner with growing  $j$ . Corresponding to the time domain, curvelets have a well-localized needle-shaped form.

For simplification, let  $\mu = (j, l, k)$  be the collection of the triple index. The system of curvelets  $(\varphi_\mu)$  forms a tight frame in  $L^2(\mathbb{R}^2)$ , i.e., each function  $f \in L^2(\mathbb{R}^2)$  can be represented by

$$f = \sum_{\mu} c_{\mu}(f) \varphi_{\mu}.$$

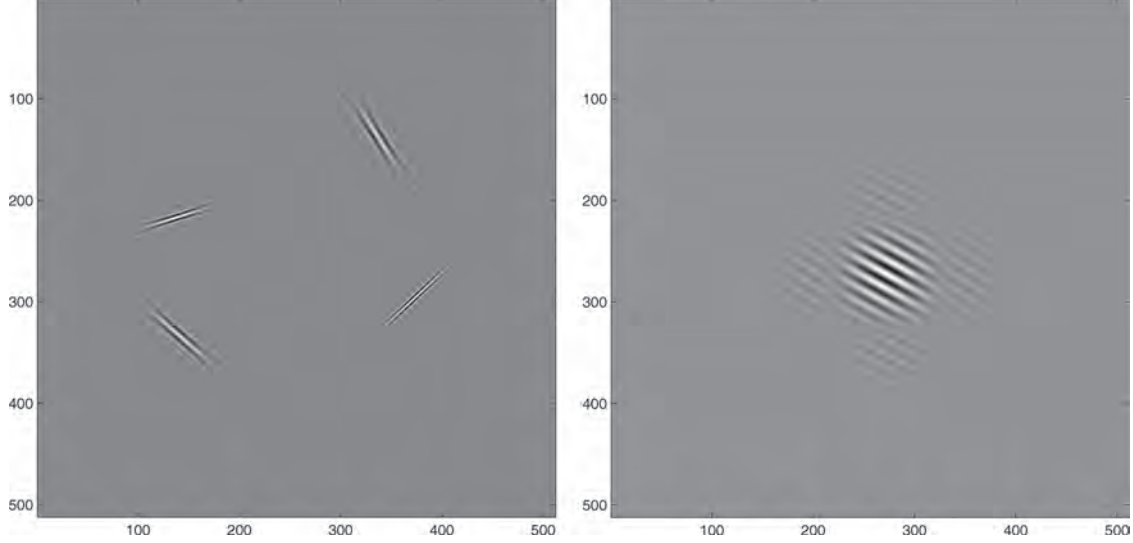


Fig. 3. Elements of (left) curvelets and (right) wave atoms in the spatial domain.

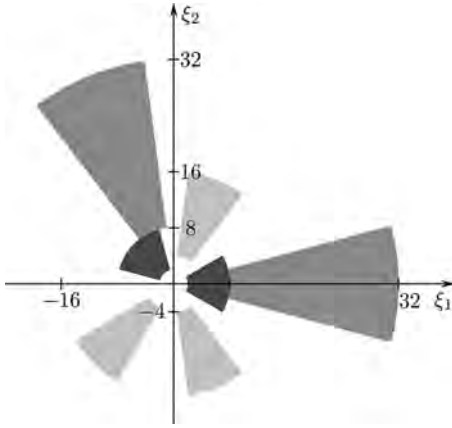


Fig. 4. Supports of frequency windows for (dark grey)  $\varphi_{2,0,k}$  and  $\varphi_{2,5,k}$ , (light grey)  $\varphi_{3,3,k}$ ,  $\varphi_{3,6,k}$  and  $\varphi_{3,13,k}$ , and (grey)  $\varphi_{4,0,k}$  and  $\varphi_{4,11,k}$ .

Using Parseval's identity, the curvelet coefficients are given by

$$\begin{aligned} c_\mu(f) &:= \langle f, \varphi_\mu \rangle = \int_{\mathbb{R}^2} \hat{f}(\xi) \overline{\hat{\varphi}_\mu(\xi)} d\xi \\ &= \int_{\mathbb{R}^2} \hat{f}(\xi) U_j(R_{\theta_{j,l}} \xi) e^{i\langle x_k^{(j,l)}, \xi \rangle} d\xi. \end{aligned} \quad (9)$$

The algorithm of forward 2-D DCuT is given as follows.

- 1) Apply a 2-D fast Fourier transform (FFT) to compute the Fourier coefficients  $\hat{f}$  of  $f$ .
- 2) Compute the product  $\hat{f}U_j$ .
- 3) Apply the inverse 2-D FFT to obtain the discrete coefficients  $c_\mu(f)$ .

The forward and inverse DCuTs have the same computational cost of  $\mathcal{O}(N^2 \log N)$  for an  $(N \times N)$  image. The redundancy of the curvelet transform is about 2.8 when wavelets are chosen at the finest scale, and 7.2 otherwise (see, e.g., [12]).

### B. Wave Atoms for Surfaces With Oriented Textures

However, curvelets are not optimal for oscillatory textures; thus, they are not good to characterize surfaces with oriented

textures, e.g., engineering surfaces by grinding, milling, polishing, and honing.

Very recently, Demanet and Ying [17] introduced the so-called wave atoms, which are a variant of 2-D wavelet packets and obey the parabolic scaling of curvelets (see Fig. 3, right). The warped oscillatory functions or oriented textures have a significantly sparser expansion in wave atoms than in other fixed standard representations like Gabor filters, wavelets, and curvelets. The texture-shape elements of wave atoms capture not only the coherence of the pattern along the oscillations like curvelets, but also the pattern across the oscillations. Fig. 3 shows the difference between the elements of the curvelets and wave atoms. The texture-shape elements of wave atoms also own very high directional sensitivity and anisotropy. Obviously, it is natural to apply the wave atoms for characterization of surfaces with oriented textures.

Let us define wave atoms as  $\varphi_\mu(x)$ , with the subscript  $\mu = (j, m, n) = (j, m1, m2, n1, n2)$  indexing a phase-space point  $(x_\mu, \omega_\mu)$  by  $x_\mu = 2^{-j}n$ ,  $\omega_\mu = \pi 2^j m$ ,  $C_1 2^j \leq \max_{i=1,2} |m_i| \leq C_2 2^j$ , where  $C_1$  and  $C_2$  are two positive constants. Then, the elements of a frame of wave packets  $\varphi_\mu$  are called wave atoms when

$$\begin{aligned} |\tilde{\varphi}_\mu(\omega)| &\leq C_M \cdot 2^{-j} (1 + 2^{-j} |\omega - \omega_\mu|)^{-M} \\ &\quad + C_M \cdot 2^{-j} (1 + 2^{-j} |\omega + \omega_\mu|)^{-M} \end{aligned} \quad (10)$$

$$|\varphi_\mu(x)| \leq C_M \cdot 2^j (1 + 2^j |x - x_\mu|)^{-M}, \quad M > 0. \quad (11)$$

The oscillations within the envelope of a wave atom in  $x$  have a wavelength  $\sim 2^{-2j}$ .

Let  $g$  be a real-valued continuous function with support included in  $[-7\pi/6, 5\pi/6]$  and such that for  $|\omega| \leq \pi/3$ ,  $g((\pi/2) - \omega)^2 + g((\pi/2) + \omega)^2 = 1$  and  $g(-(\pi/2) - 2\omega) = g((\pi/2) + \omega)$ . Define  $v$  as the inverse Fourier transform  $v(t) = (2\pi)^{-1} \int g(\omega) e^{i\omega t} d\omega$ , and

$$\psi_m^0(t) = 2Re \left\{ e^{i\pi(m+\frac{1}{2})t} v \left( (-1)^n \left( t - \frac{1}{2} \right) \right) \right\}. \quad (12)$$

The Fourier transform of  $\psi_m^0$  is given by [17], [49]

$$\hat{\psi}_m^0(\omega) = e^{-i\omega/2} \left[ e^{i\alpha_m} g \left( \epsilon_m \left( \omega - \pi \left( m + \frac{1}{2} \right) \right) \right) + e^{-i\alpha_m} g \left( \epsilon_{m+1} \left( \omega + \pi \left( m + \frac{1}{2} \right) \right) \right) \right]. \quad (13)$$

Here,  $\epsilon_m = (-1)^m$ ,  $\alpha_m = (\pi/2)(m + (1/2))$ , and  $\sum_m |\hat{\psi}_m^0(\omega)|^2 = 1$ .

Write basis functions as  $\psi_{m,n}^j(x) = \psi_m^j(x - 2^{-j}n) = 2^{j/2} \psi_m^0(2^j x - n)$ . Then, coefficients of the transform can be obtained by

$$c_{j,m,n} = \int \psi_{m,n}^j(x) f(x) dx = \frac{1}{2\pi} \int e^{i2^{-j}n\omega} \overline{\hat{\psi}_m^j(\omega)} \hat{f}(\omega) d\omega. \quad (14)$$

Assuming that the function is discretized at  $x_k = kh$ ,  $h = 1/N$ ,  $k = 1, \dots, N$ , we have

$$c_{j,m,n} \simeq \frac{1}{2\pi} \sum_{k=2\pi(-N/2+1:1:N/2)} e^{i2^{-j}nk} \overline{\hat{\psi}_m^j(k)} \hat{f}(k). \quad (15)$$

The 2-D extension can be formed by the following products:

$$\begin{aligned} \varphi_\mu^+(x_1, x_2) &= \psi_{m_1}^k(x_1 - 2^{-j}n_1) \psi_{m_2}^k(x_2 - 2^{-j}n_2) \\ \varphi_\mu^-(x_1, x_2) &= H\psi_{m_1}^k(x_1 - 2^{-j}n_1) H\psi_{m_2}^k(x_2 - 2^{-j}n_2) \end{aligned}$$

where  $H$  is the Hilbert transform. The combinations  $\varphi_\mu^{(1)} = (\varphi_\mu^+ + \varphi_\mu^-)/2$  and  $\varphi_\mu^{(2)} = (\varphi_\mu^+ - \varphi_\mu^-)/2$  form the wave atom frame and be denoted jointly as  $\varphi_\mu$  [17].

The algorithm can be implemented by the following three steps: 1) Apply 2-D FFT for  $f(x_k)$ ; 2) wrap the product  $\hat{\psi}_m^j \hat{f}$  by periodicity inside the interval  $[-2^j\pi, 2^j\pi]$  for each  $(j, m)$ ; and 3) perform the inverse 2-D FFT. The computational complexity of wave atom transform is  $\mathcal{O}(N^2 \log N)$ .

#### IV. DECODE: NONLINEAR SPARSE RECOVERY

In the last two years, a few iterative algorithms, e.g., orthogonal matching pursuit [48], gradient projection [24], and iterative thresholding algorithms [3], [15], [16], [25], [42], have been proposed by mathematicians to exactly reconstruct the  $x$  in (1) or  $\vartheta$  in (2). In this paper, we follow the way of iterative thresholding since this methodology is considerably robust and simple to be implemented. In particular, the iterative curvelet thresholding and wave atom thresholding are applied for surfaces with scratches and textures, respectively.

Related algorithms on iterative thresholding have been presented for constrained optimization problems by a few researchers (see, e.g., [15], [16], [25], and [42]). For instance, Daubechies *et al.* [15] presented an iterative thresholding algorithm for wavelet regularization (i.e., inverse problem with wavelet sparse constrains). However, in this seminal paper, the problems of undersampling or partial measuring were not considered. Peyré [42] proposed iterative thresholding with best

basis constrains for CS to recover images. We observed that the iterative thresholding is quite related to nonlinear inverse diffusion or the so-called inverse scale space method [51]. We will describe the connections between our proposed method with the inverse diffusion equation elsewhere.

Let us have a look at the motivation of the iterative thresholding for recovery of linear inverse problems. If without undersampling (i.e.,  $\Phi \in \mathcal{C}^{N,N}$ ), one can recover  $x$  by  $x = \Phi^{-1}y - \Phi^{-1}\epsilon$ . Very frequently,  $\Phi$  corresponds to a low-pass filtering so that  $\Phi^{-1}\epsilon$  magnifies the noises, which leads to an ill-posed inverse problem. The iterative thresholding essentially deals with the inverse problem as an iterative denoising. In fact, the iterative thresholding was initially presented as an expectation-maximization algorithm for image deconvolution [24]. Convergence of iterative thresholding algorithm can be found in [15]. The algorithm only requires matrix-vector multiplications of  $\Phi$  and  $\Phi^T$ , and it is based on bounding the matrix  $\Phi^T\Phi$  by a diagonal matrix  $D$  (i.e.,  $D - \Phi^T\Phi$  is positive semidefinite), and thus, the solution of (3) can be obtained by a sequence of simpler denoising. A wide-angle review of iterative thresholding algorithms involving denoising, deconvolution, and CS can be found in [23].

Define the following thresholding function:

$$S_\tau(f, \Psi) = \sum_\mu \tau(c_\mu(f)) \varphi_\mu \quad (16)$$

where  $\tau$  can be taken as a soft-thresholding function defined by a fixed threshold  $\sigma > 0$ , i.e.,

$$\tau_s(x) = \begin{cases} x - \sigma, & x \geq \sigma \\ 0, & |x| < \sigma \\ x + \sigma, & x \leq -\sigma \end{cases}$$

or a hard-thresholding function, i.e.,

$$\tau_h(x) = \begin{cases} x, & |x| \geq \sigma \\ 0, & |x| < \sigma \end{cases}$$

or the continuous garrote thresholding, i.e.,

$$\tau_g(x) := \begin{cases} x - \frac{\sigma^2}{x}, & |x| \geq \sigma \\ 0, & |x| < \sigma \end{cases}$$

which may be a good choice where large coefficients nearly remain unaltered.

By solving a minimization of surrogate function [15], [42], one can obtain the solution by iterating the thresholding function, i.e.,

$$S_\tau(x + \Phi^T(y - \Phi x), \Psi). \quad (17)$$

Outline the algorithm as follows.

- 1) Initialization: set the iterative number  $p = 0$  and initial value  $x_0 = 0$  or a zero-filling reconstruction by interpolating zeros for missed samples [30].
- 2) Update the estimation

$$\tilde{x}_p = x_p + \Phi^T(y - \Phi x_p).$$

3) Apply curvelet/wave atom thresholding for the estimation

$$x_{p+1} = S_\tau(\tilde{x}_p, \Psi).$$

- 4) Iteration: if  $\|x_{p+1} - x_p\| > \varepsilon$ , then set  $p + 1$  to  $p$  and go to step 2; otherwise, stop iterations.
- 5) Alternatively, in the last several iterations or after all iterations, one can apply total variation (TV)-synthesis y curvelet/wave atom thresholding [35], [38], which can suppress the pseudo-Gibbs artifacts (small high-frequency oscillatory due to false reconstruction of fine-scale coefficient components) and element-like artifacts while preserving the discontinuous edges and features. Here, the TV of a function  $f$  with  $|\nabla f \in L^1(\Omega)|$  is defined by  $\text{TV}(f) = \int_\Omega |\nabla f(\zeta)| d\zeta$  [45]. The thresholding is posed as an optimization problem involving the total variation norm and a constraint on the curvelet space. It can be interpreted as a projected iterative thresholding. Essentially, the TV minimization keeps the significant coefficients unchanged and does not set the insignificant coefficients to zero as conventional shrinkage does but typically makes it optimal small to eliminate the artifacts.

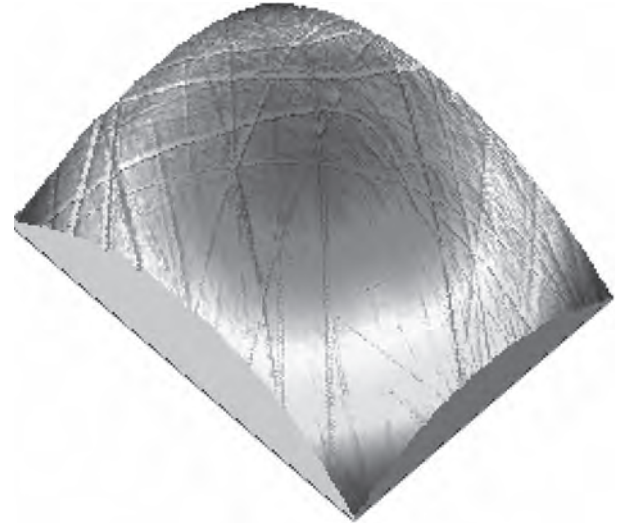
The threshold value  $\sigma$  is dependent on practical problems. The question on how to choose the  $\sigma$  optimally for specific metrology is open. Normally, one can use a uniform threshold value or an updating threshold value through iterations. Recently, the iterative curvelet thresholding has also been applied to deblurring problems with highly incomplete measurements in the field of remote sensing [41].

The iterative thresholding produces a sequence of inverse scale space, which starts from the measurement data (or an initial value with zeros) and approaches the real surfaces as iteration increases. If we use linear decaying threshold values, the produced recovery sequence changes from smooth space to fine space. If the iteration is stopped at a suitable time, large-scale features may already be incorporated into the reconstruction, while fine-scale features are still missing.

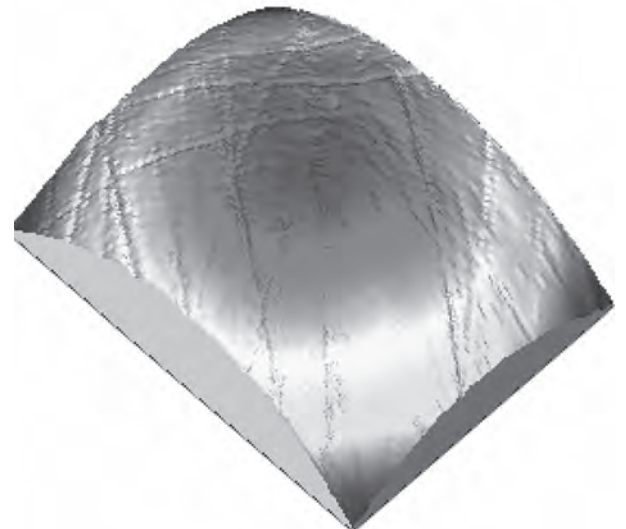
It should be noted that one can apply orthogonal wavelets in this framework for surfaces with point features. A nonlinear conjugate gradient has been used for such a wavelet case in medical magnetic resonance imaging [30].

## V. NUMERICAL EXPERIMENTS

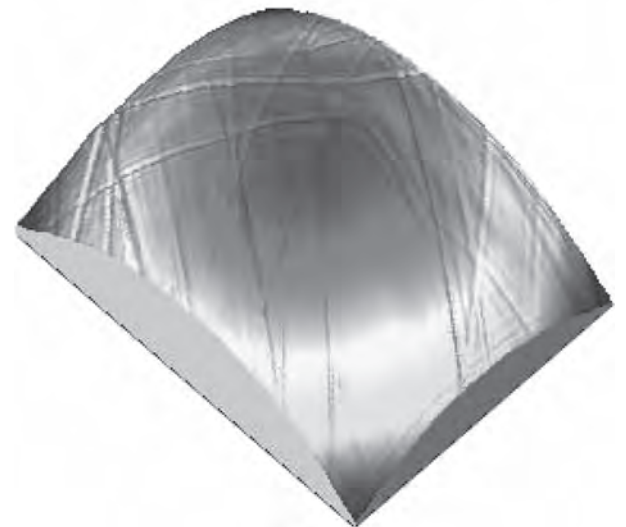
Real surfaces are naturally compressible by suitable coding in an appropriate transform domain. For example, surfaces with peaks/pits are sparse in the wavelet domain, and surfaces with straight scratches are compressible in the ridgelet domain [34], while surfaces with curve scratches have better compressible in the curvelet domain. So far, the sparse representation and decomposition of engineering surfaces has been addressed much in the literature (see, e.g., [13], [28], [29], [32], [34]–[36], and [44]). Fig. 5(a) shows a typical example: a worn metallic femoral head of biomedical orthopedic implant. This surface has a sparse representation in the wavelet frame domain. Fig. 5(b) and (c) presents the partial reconstruction using the largest 1% wavelet and curvelet coefficients. The



(a)



(b)



(c)

Fig. 5. Partially sparse reconstruction of a raw surface topography measured from a metallic joint head implant. (a) Original surface. (b) Reconstructed surface by 1% largest wavelet coefficients. (c) Reconstructed surface by 1% largest curvelet coefficients.

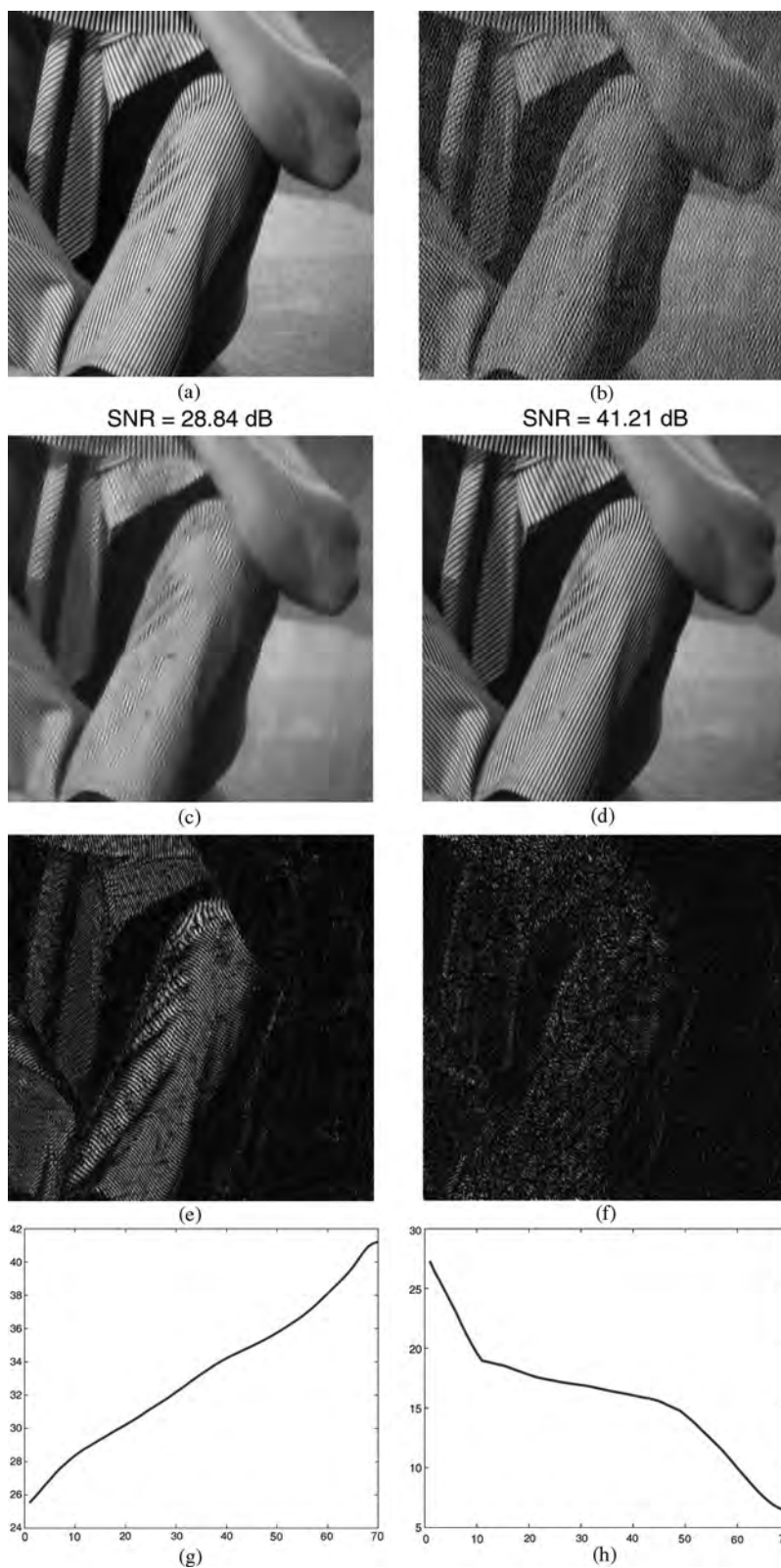


Fig. 6. Compressed measurement for a standard textural data. (a) Original data. (b) Zero-filling reconstruction. (c) *Wavelet-TV* recovery. (d) Recovery by the proposed method. (e) and (f) Removed components by (c) and (d). (g) and (h) SNR and recovery errors versus number of iterations. The horizontal coordinate in (g) and (h) denotes the number of iterations, and the vertical coordinate denotes SNR in (g) and recovery errors in (h).

curvelet partial reconstruction has better performance than wavelet reconstruction. Curvelet transform preserves the edges of scratches, while the wavelet transform results in oscillation artifacts along the edges. The good compressibility of surfaces

in the directional wavelet domain makes it possible to apply the CS for surface metrology.

In the first example, we apply the proposed compressed measurement method for a “Lena” image that is a standard

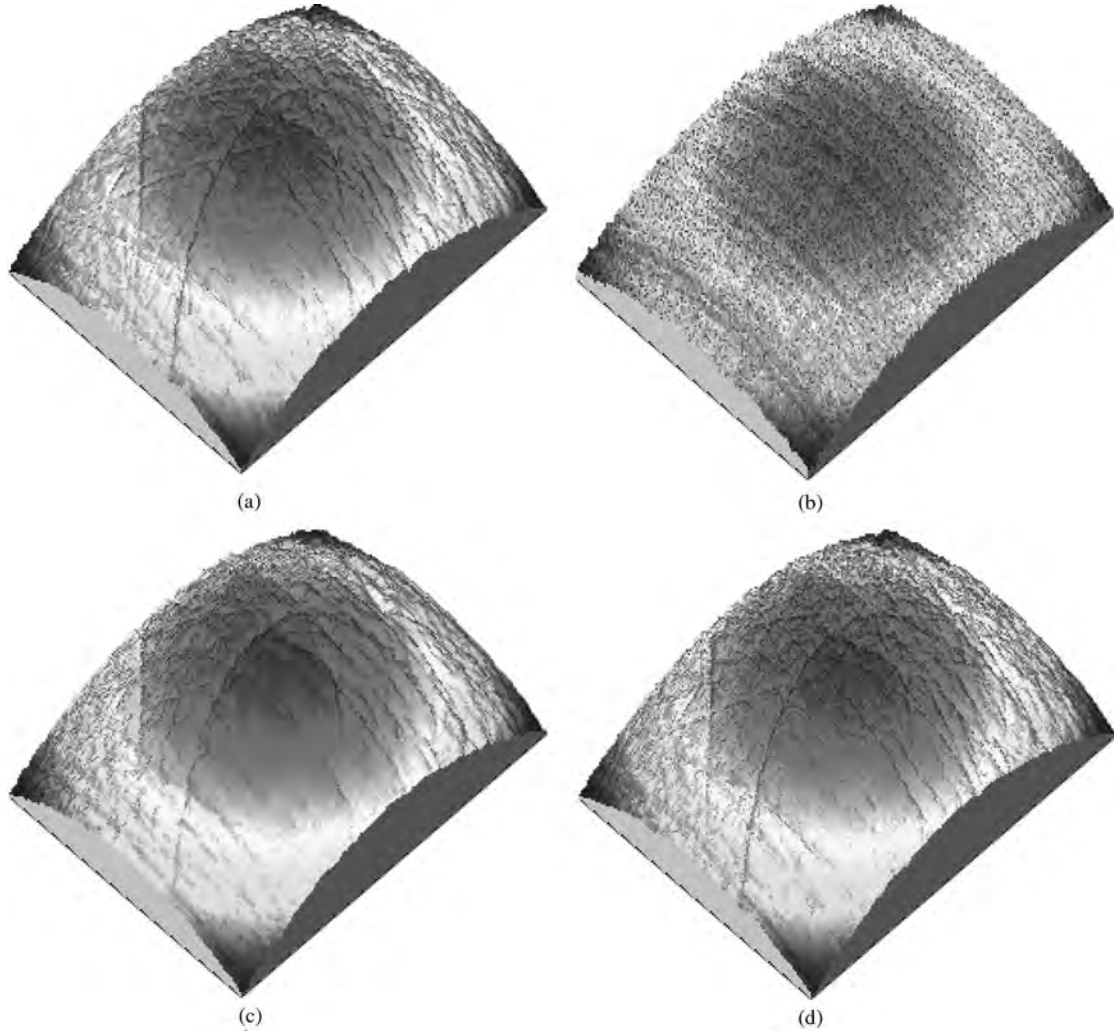


Fig. 7. Compressed measurement for a raw joint surface. (a) Original surface. (b) Zero-filling reconstruction. (c)  $l_1 - TV$  recovery. (d) recovery by the proposed method.

textural data. Fig. 6(a) shows the original data. We consider the 25% partial random measurement in the Fourier space [30]. The measurement sampling strategy will be emphasized at the end of this section. Fig. 6(b) is a zero-filling reconstruction from the incomplete  $K$ -space measurement. Fig. 6(c) is obtained using *wavelet-TV* recovery, i.e., solving minimization of  $\|\vartheta\|_{l_1} + TV(x)$ , subject to  $\|\hat{A}\vartheta - y\| \leq \epsilon$  by a nonlinear conjugate gradient method [30]. The signal-to-noise ratio (SNR) achieved is 28.84 dB. Fig. 6(d) is the recovery data using our iterative curvelet thresholding, where we take the zero-filling reconstruction as an initial data and use a linear decaying threshold value  $\sigma_0(1 - n/M)$ , in which  $M = 70$  is the total number of iterations,  $n$  is an index of iterations, and the initial threshold  $\sigma_0 = 0.05$ . The SNR of the recovered image is 41.21 dB. Fig. 6(e) shows the lost components (i.e., the difference between the recovery and original data) by the *wavelet-TV* method. Fig. 6(f) shows the lost components by the proposed method. It can clearly be seen that the proposed method recovers the edges and textures much better than other methods. Fig. 6(g) shows the changes in the SNR as the number of iterations increases, and Fig. 6(h) shows the changes of  $l_1$ -norm errors between the recovery

and original data (i.e.,  $\|x - x_0\|_{l_1}$ ) as the number of iterations increases.

After the encouraging results on modeling examples, we show the abilities of the proposed method to extract and recover scratches from microscaler surfaces of biomedical implanted joints. The metrology of the surfaces is related to biological compatibility and life expectancy of joints. Fig. 7(a) displays a raw surface topography from a worn metallic joint head with morphological structures consisting of roughness and deep scratches. The sampling interval in the horizontal  $x$ - and  $y$ -directions of the surface is 0.952 and 0.817  $\mu\text{m}$ , and that in the vertical direction is 1  $\mu\text{m}$ . The number of sampling points is  $240 \times 368$ . We again use the  $K$ -space random measurement matrix. Fig. 7(b) is the zero-filling reconstruction, and Fig. 7(c) is the  $l_1$ -TV reconstruction, i.e., solving the minimization of  $\|x\|_{l_1} + TV(x)$ , subject to  $\|\Phi x - y\| \leq \epsilon$  [6], [30]. Fig. 7(d) is the recovery by our iterative curvelet thresholding. Again, we show the performance of the proposed method for a surface measured from another worn femoral head of orthopedic implant shown in Fig. 8(a). Fig. 8(b)–(d) is obtained by zero-filling reconstruction,  $l_1$ -TV, and our iterative curvelet thresholding, respectively. Our method recovers the scratches very well. It

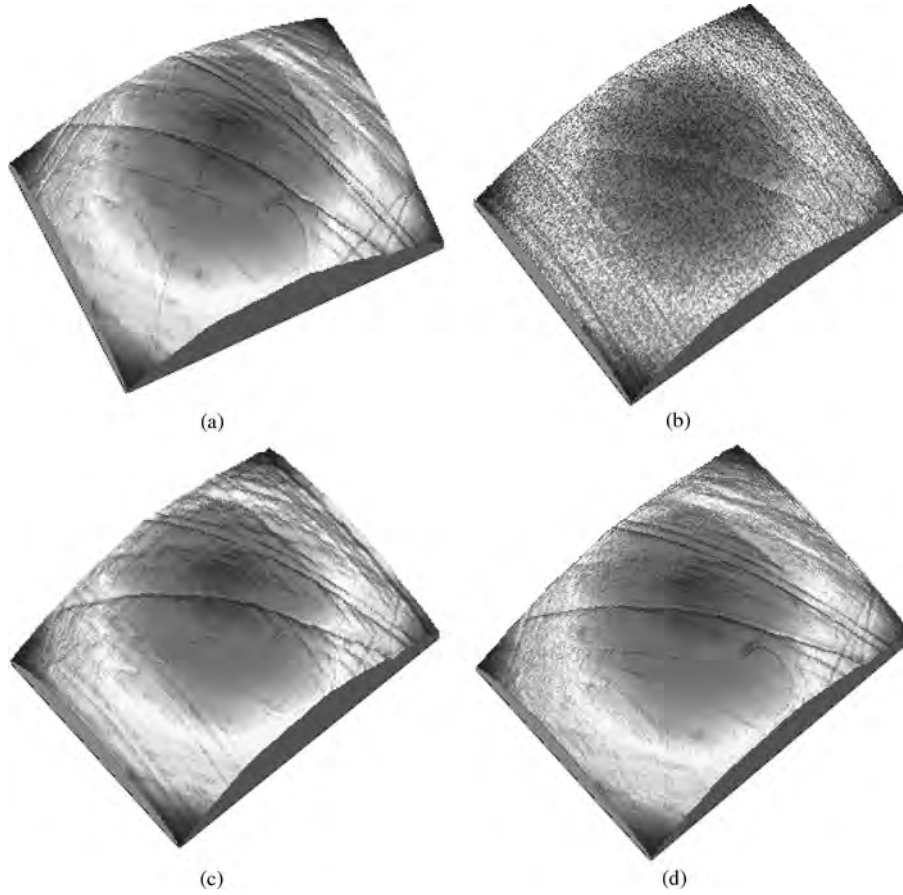


Fig. 8. (a) original surface. (b) zero-filling reconstruction. (c)  $l_1$ -TV recovery. (d) Recovery by the proposed method.

should be noted that a  $K$ -space measurement noise (produced by 0.05 times of random numbers) is considered in the two tests above.

Other engineering surfaces are also considered. Fig. 9(a) shows a honed surface of an automotive engine cylinder. The sampling interval in the horizontal  $x$ - and  $y$ -directions of the surface is 16 and 16  $\mu\text{m}$ , and that in the vertical direction is 5.3  $\mu\text{m}$ . The surface including the form, waviness, and roughness components that almost submerge the main features of the deep valleys or pits. Usually, the most important features that affect the performance of the cylinder are deep valleys whose distribution and amplitude will considerably influence the flow of gas or air in a pressure balance of an engine. Detection of these features is also useful for online manufacture monitoring. Fig. 9(b) and (c) is recovered by zero-filling reconstruction and iterative curvelet thresholding. We see that the proposed method can recover the surfaces almost exactly from the incomplete measurement. Fig. 9(d) is obtained to extract the deep valleys directly from compressed measurement for morphological assessment by the iterative curvelet thresholding using an experiential threshold value. Here, we want to show that it is also possible to directly extract scratched features (e.g., by using suitable thresholding) for metrology from the highly incomplete random measurements without the need to recover the full original surface first.

Now, we show the ability of the compressed measurement based on the wave atom transform. Fig. 10(a) shows a very

noise surface. We consider measurement noises at the same time. The sampling interval in the horizontal  $x$ - and  $y$ -directions of the surface is 6.6 and 7.7  $\mu\text{m}$ , and that in the vertical direction is 1.2  $\mu\text{m}$ . The number of sampling points is  $256 \times 256$ . Fig. 10(b) is the *wavelet-TV* recovery. Fig. 10(c) and (d) shows the surface with extracted scratches by curvelet thresholding with 30 iterations and wave atom thresholding with five iterations. Wave atoms are more sparse for such a textural surface. The proposed compressed measurement methods are robust for surfaces with noise and measurement errors.

Finally, it should be emphasized that random point undersampling with a factor of 0.25 (i.e., 25% measurements) from a Cartesian grid in Fourier measurement space has been applied in the above experiments. The Fourier measurements can easily be implemented by existing optical imaging instruments. Fig. 11 shows an example for the sampling pattern with its sampling probability density function. Various measurement numbers would result in different accuracy and convergence to some extent. Taking the honed surface (shown in Fig. 9) as an example, Fig. 12 shows the comparisons of SNR and  $l_1$ -norm recovery errors as the number of iterations increases by using undersampling measurement with a factor of 0.25 (shown as a real line) and with a factor of 0.1 (shown as a dashed line).

Furthermore, Fig. 13 is an example showing how the accuracy of the retrieved surface is influenced, depending on the number of samples, and showing when the proposed method fails. Fig. 13 shows the changes of SNR and recovery errors

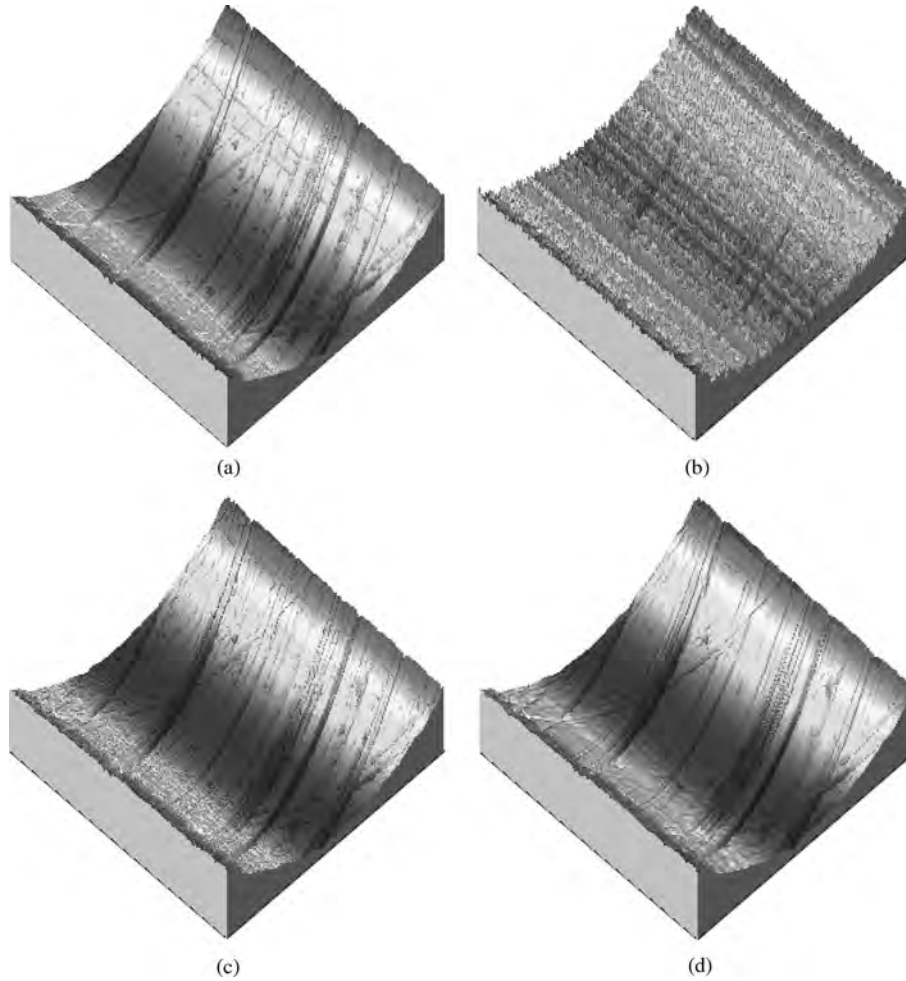


Fig. 9. Compressed measurement for a honed surface of the automotive engine cylinder. (a) Original surface. (b) Zero-filling reconstruction. (c) Iterative curvelet thresholding using linear decaying threshold values from the maximum value to zero. (d) Iterative curvelet thresholding using a suitable threshold values that does not tend to zero.

as the number of measurements increases from 10% samples to 55% samples. The upper row shows the results by using the iterative curvelet thresholding with 30 iterations and  $\sigma_0 = 0.06$ . It can be seen clearly that the minimum number of measurements for this case is 30% of the samples so as to obtain a satisfying recovery sequence. The lower row shows the results by using 50 iterations, where the case with 20% measurements is also a satisfying point. Results are mainly related to measurement matrices in the encoding step and parameters of the recovery algorithm in the decoding step. Because the random measurement strategy is used in our experiments, the measurement matrix is different for each implementation, which also leads to a slight different recovery to some extent. Normally, one can use less iterative times for a case with more measurements. Once a safe or quality-guaranteed number of measurements is used, the proposed method can balance the cost of encode and decode according to our practical requirements.

Other sampling trajectories, such as parallel-line, radial-line, or spiral sampling, can also be applied for the compressed measurement [31]. Furthermore, variable-density sampling can be used to match the nonuniform energy distribution of surfaces in the Fourier space. These complex sampling trajectories are irregular in a non-Cartesian grid, which involves nonequispaced

Fourier transform. The choice of trajectory is application dependent, where one has to consider surface characteristics and instrumental considerations. In practice, we can choose the sampling trajectories or measurement strategy obeying the following rule: 1) There should be lower coherence to sparse basis; 2) it should be easily implemented by measurement instruments; and 3) a fast nonlinear recovery algorithm can be applied for this sampling trajectory.

## VI. CONCLUSION

This paper has considered a problem of surface metrology with highly incomplete measurements. The novelty of this paper includes the following two aspects.

- 1) A compressed measurement mechanism for surface metrology was proposed, inspired by a new concept named compressive sampling from information theorem, which is used to solve undetermined ill-posed inverse problems. The compressed metrology enables us to accurately and robustly recover surfaces from an incomplete set of measurements dictated by geometric and structured features, rather than its Fourier bandwidth limited by the Shannon sampling theorem. In particular, one only needs

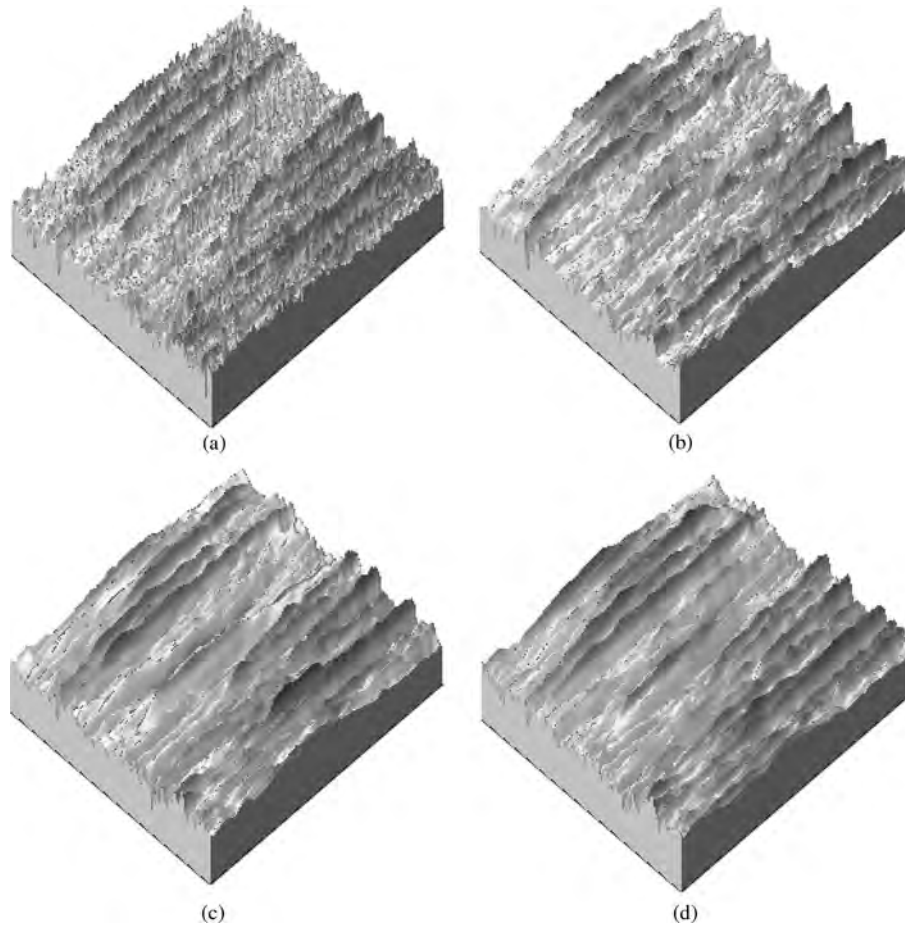


Fig. 10. Compressed metrology for a noise microscaler engineering surface. (a) Original surface. (b) *Wavelet-TV* recovery. (c) Iterative curvelet thresholding with 30 iterations. (d) Iterative wave atom thresholding with five iterations.

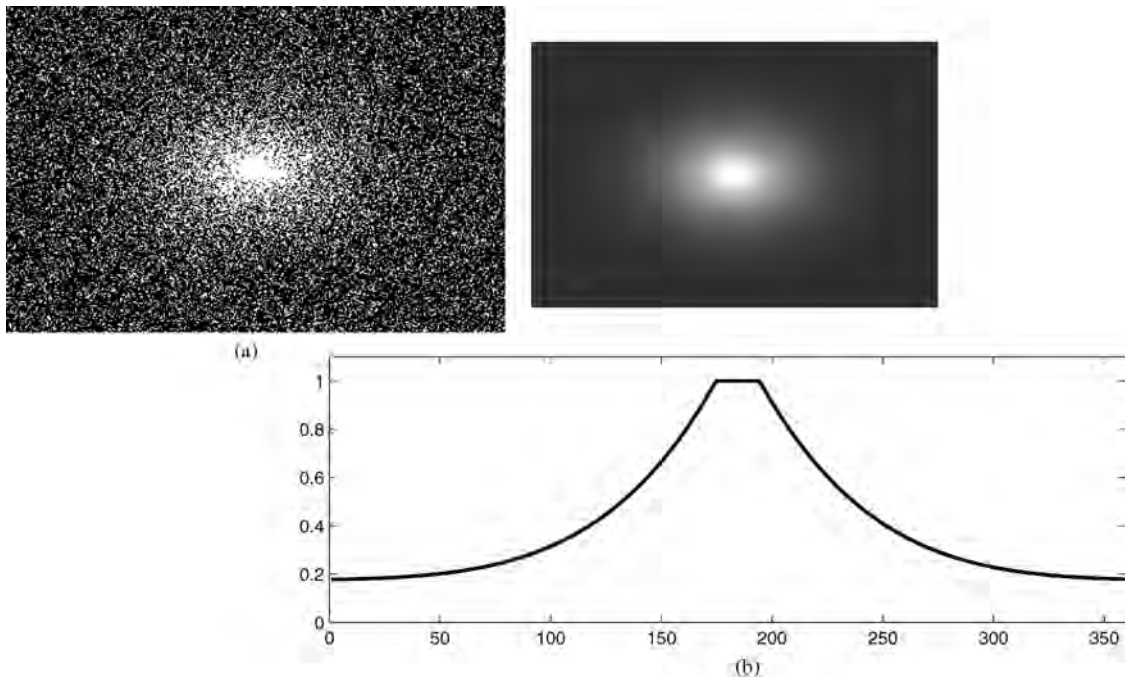


Fig. 11. Random point undersampling with a factor of 0.25 from a Cartesian grid in the Fourier measurement space. (a) Sampling pattern (the white points denotes sampling points). (b) Sampling probability density function (the upper subfigure is its 2-D density function and the lower subfigure is its 1-D center profile, and the horizontal coordinate denotes the sample).

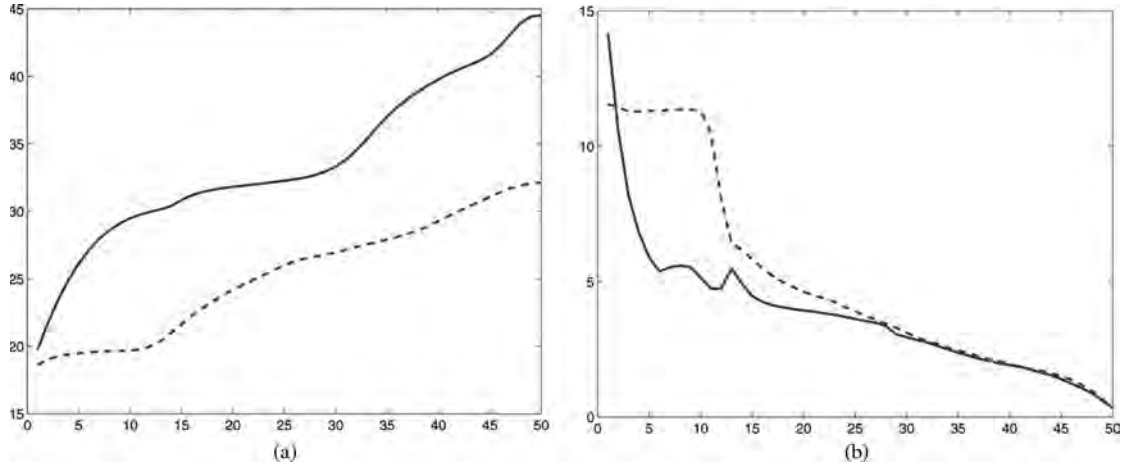


Fig. 12. Comparisons of (a) SNR and (b)  $l_1$ -norm errors as iterative number increases using different undersampling factors for the honed surface of an automotive engine cylinder. The real line denotes the case using 25% measurements, and the dashed line denotes 10% measurements. The horizontal coordinate denotes the number of iterations. The vertical coordinate denotes the value of SNR in (a) and recovery errors in (b).

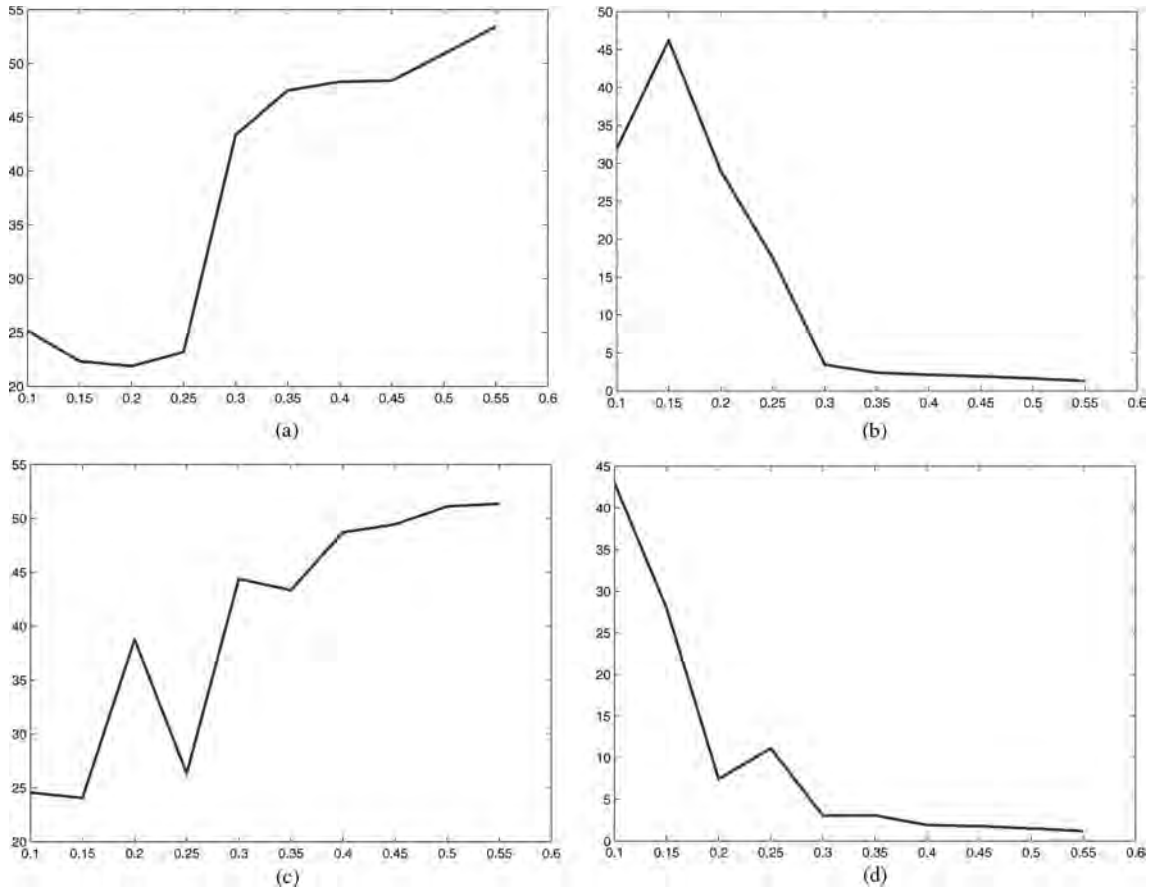


Fig. 13. (a) and (c) SNR versus number of measurements (or sampling points). (b) and (d) Recovery errors versus number of measurements. The horizontal coordinate denotes the ratio of number of measurements. The vertical coordinate denotes the value of SNR in (a) and (c) and recovery errors in (b) and (d). The iterative curvelet thresholding with 30 iterations has been used for recovery in the upper row and with 50 iterations in the lower row.

$O(S \cdot \log(N/S))$  random measurement to recover an  $S$ -sparse  $N \times N$  surface.

- 2) A convex-optimization solution with multiscale and multidirectional sparse constrains was provided for non-linear recovery of the compressed measurements using iterative curvelet/wave atom thresholding methods. The proposed methods are particularly suitable for surfaces with scratches and textures.

The CS makes us to rethink sensing mechanisms for surface metrology. If surfaces are compressible in an appropriate transform domain, we can design a sensing mechanism that are low incoherent to this transform to sparsely measure the surfaces. The technique can be applied to various instruments, such as the stylus, CT, and SEM, and would be significant for ongoing applications for precision engineering involving metrology, tribology, physics, and medical and biological engineering.

Finally, we present the following new directions and open problems for compressed measurements in future research.

- 1) How can we design an optimal sampling scheme with low-rate incoherent measurements for numerous real surfaces?
- 2) How can we design CS measurement devices (e.g., an optical imaging system) according the sampling scheme that directly records compressed patterns for practical applications?
- 3) Can we implement the wavelet transform or curvelet transform by an optical measurement system? Can we consider the sparse measurement in wavelet domain instead of Fourier domain?
- 4) How can we speed up the decoding recovery algorithm?
- 5) How can we estimate roughness parameters ( $R_a$ ,  $R_q$ ,  $R_v$ , etc.) directly from the compressed measurements while do not need to recover full surface first?

#### ACKNOWLEDGMENT

The author would like to thank the editors and referees for their constructive suggestions, which substantially improved this paper, L. Blunt, X. Jiang, and P. Scott of the Center for Precision Technology at the University of Huddersfield (U.K.) for the previous discussions on surface metrology, A. Antoniadis of the University of Joseph Fourier (France), and G. Plonka of the University of Duisburg-Essen (Germany) for the stimulating discussions on curvelets.

#### REFERENCES

- [1] A. Antoniadis and J. Fan, "Regularization of wavelet approximation," *J. Amer. Stat. Assoc.*, vol. 96, no. 455, pp. 939–967, Sep. 2001.
- [2] R. Baraniuk, "A lecture on compressive sensing," *IEEE Signal Process. Mag.*, vol. 24, no. 4, pp. 118–121, Jul. 2007.
- [3] T. Blumensath and M. E. Davies, "Iterative thresholding for sparse approximations," *J. Fourier Anal. Appl.*, vol. 14, no. 5/6, pp. 629–654, Dec. 2008.
- [4] C. Brown, W. Johnsen, and K. Hult, "Scale-sensitivity, fractal analysis and simulations," *Int. J. Mach. Tools Manuf.*, vol. 38, no. 5/6, pp. 633–637, May/Jun. 1998.
- [5] E. J. Candès and T. Tao, "Decoding by linear programming," *IEEE Trans. Inf. Theory*, vol. 51, no. 12, pp. 4203–4215, Dec. 2005.
- [6] E. J. Candès, J. Romberg, and T. Tao, "Stable signal recovery from incomplete and inaccurate information," *Commun. Pure Appl. Math.*, vol. 59, no. 8, pp. 1207–1233, Aug. 2006.
- [7] E. J. Candès and T. Tao, "Near optimal signal recovery from random projections: Universal encoding strategies," *IEEE Trans. Inf. Theory*, vol. 52, no. 12, pp. 5406–5425, Dec. 2006.
- [8] E. J. Candès, J. Romberg, and T. Tao, "Robust uncertainty principles: Exact signal reconstruction from highly incomplete frequency information," *IEEE Trans. Inf. Theory*, vol. 52, no. 2, pp. 489–509, Feb. 2006.
- [9] E. J. Candès, "Compressive sampling," in *Proc. Int. Congr. Mathematicians*, Madrid, Spain, 2006, vol. 3, pp. 1433–1452.
- [10] E. J. Candès and M. B. Wakin, "An introduction to compressive sampling," *IEEE Signal Process. Mag.*, vol. 25, no. 2, pp. 21–30, Mar. 2008.
- [11] E. J. Candès and D. L. Donoho, "New tight frames of curvelets and optimal representations of objects with piecewise  $C^2$  singularities," *Commun. Pure Appl. Math.*, vol. 57, no. 2, pp. 219–266, Feb. 2004.
- [12] E. J. Candès, L. Demanet, D. L. Donoho, and L. Ying, "Fast discrete curvelet transforms," *Multiscale Model. Simul.*, vol. 5, no. 3, pp. 861–899, Jan. 2006.
- [13] X. Chen, J. Raja, and S. Simanapalli, "Multi-scale analysis of engineering surfaces," *Int. J. Mach. Tools Manuf.*, vol. 35, no. 2, pp. 231–238, Feb. 1995.
- [14] I. Daubechies, *Ten Lectures on Wavelets*. Philadelphia, PA: SIAM, 1992.
- [15] I. Daubechies, M. De Fries, and C. De Mol, "An iterative thresholding algorithm for linear inverse problems with a sparsity constraint," *Commun. Pure Appl. Math.*, vol. 57, no. 11, pp. 1413–1457, Nov. 2004.
- [16] I. Daubechies, M. Fornasier, and I. Loris, "Accelerated projected gradient method for linear inverse problems with sparsity constraints," *J. Fourier Anal. Appl.*, vol. 14, no. 5/6, pp. 764–792, Dec. 2008.
- [17] L. Demanet and L. Ying, "Wave atoms and sparsity of oscillatory patterns," *Appl. Comput. Harmon. Anal.*, vol. 23, no. 3, pp. 368–387, Nov. 2007.
- [18] R. De Vore, "Deterministic constructions of compressed sensing matrices," *J. Complex.*, vol. 23, no. 4–6, pp. 918–925, Aug. 2007.
- [19] M. Do and M. Vetterli, "The contourlet transform: An efficient directional multiresolution image representation," *IEEE Trans. Image Process.*, vol. 14, no. 12, pp. 2091–2106, Dec. 2005.
- [20] D. Donoho, "Compressed sensing," *IEEE Trans. Inf. Theory*, vol. 52, no. 4, pp. 1289–1306, Apr. 2006.
- [21] M. Duarte, M. Davenport, D. Takhar, J. Laska, T. Sun, K. Kelly, and R. Baraniuk, "Single-pixel imaging via compressive sampling," *IEEE Signal Process. Mag.*, vol. 25, no. 2, pp. 83–91, Mar. 2008.
- [22] M. Elad, "Optimized projections for compressed sensing," *IEEE Trans. Signal Process.*, vol. 55, no. 12, pp. 5695–5702, Dec. 2007.
- [23] M. Elad, B. Matalon, J. Shtok, and M. Zibulevsky, "A wide-angle view at iterated shrinkage algorithms," in *Proc. SPIE—Wavelet XII*, San Diego, CA, Aug. 2007, vol. 6701, p. 670 102.
- [24] M. Figueiredo, R. Nowak, and S. Wright, "Gradient projection for sparse reconstruction: Application to compressed sensing and other inverse problems," *IEEE J. Sel. Topics Signal Process.*, vol. 1, no. 4, pp. 586–597, Dec. 2007.
- [25] M. Fornasier and H. Rauhut, "Iterative thresholding algorithms," *Appl. Comput. Harmon. Anal.*, vol. 25, no. 2, pp. 187–208, Sep. 2008.
- [26] G. Kaiser, *A Friendly Guide to Wavelets*. Boston, MA: Birkhauser, 1994.
- [27] P. Indyk, "Explicit constructions for compressed sensing of sparse signals," in *Proc. 19th Symp. Discr. Algorithms*, 2008, pp. 30–33.
- [28] X. Jiang, L. Blunt, and K. J. Stout, "Development of a lifting wavelet representation for surface characterization," *Proc. R. Soc. Lond. A, Math. Phys. Sci.*, vol. 456, no. 2001, pp. 2283–2313, Sep. 2000.
- [29] B. Josso, D. Burton, and M. Lalor, "Wavelet strategy for surface roughness analysis and characterization," *Comput. Methods Appl. Mech. Eng.*, vol. 191, no. 8–10, pp. 829–842, Dec. 2001.
- [30] M. Lustig, D. Donoho, and J. Pauly, "Sparse MRI: The application of compressed sensing for rapid MR imaging," *Magn. Reson. Med.*, vol. 58, no. 6, pp. 1182–1195, Dec. 2007.
- [31] M. Lustig, D. Donoho, J. Santos, and J. Pauly, "Compressed sensing MRI," *IEEE Signal Process. Mag.*, vol. 25, no. 2, pp. 72–82, Mar. 2008.
- [32] J. Ma, X. Jiang, and P. Scott, "Complex ridgelets for shift invariant characterization of surface topography with line singularities," *Phys. Lett. A*, vol. 344, no. 6, pp. 423–431, Sep. 2005.
- [33] J. Ma, "Towards artifact-free characterization of surface topography using complex wavelets and total variation minimization," *Appl. Math. Comput.*, vol. 170, no. 2, pp. 1014–1030, Nov. 2005.
- [34] J. Ma and M. Fenn, "Combined complex ridgelet shrinkage and total variation minimization," *SIAM J. Sci. Comput.*, vol. 28, no. 3, pp. 984–1000, 2006.
- [35] J. Ma, "Curvelets for surface characterization," *Appl. Phys. Lett.*, vol. 90, no. 5, p. 054 109, Jan. 2007.
- [36] J. Ma, "Characterization of textural surfaces using wave atoms," *Appl. Phys. Lett.*, vol. 90, no. 26, p. 264 101, Jun. 2007.
- [37] J. Ma, A. Antoniadis, and F.-X. Le Dimet, "Curvelet-based snake for multiscale detection and tracking of geophysical fluids," *IEEE Trans. Geosci. Remote Sens.*, vol. 44, no. 12, pp. 3626–3638, Dec. 2006.
- [38] J. Ma and G. Plonka, "Combined curvelet shrinkage and nonlinear anisotropic diffusion," *IEEE Trans. Image Process.*, vol. 16, no. 9, pp. 2198–2206, Sep. 2007.
- [39] J. Ma and G. Plonka, "A review of curvelets and recent applications," *IEEE Signal Process. Mag.*, 2009, to be published.
- [40] J. Ma and G. Plonka, "Computing with curvelets: From image processing to turbulent flows," *IEEE Comput. Sci. Eng.*, vol. 11, no. 2, pp. 72–80, Mar./Apr. 2009.
- [41] J. Ma and F.-X. Le Dimet, "Deblurring from highly incomplete measurements for remote sensing," *IEEE Trans. Geosci. Remote Sens.*, vol. 47, no. 3, pp. 792–802, Mar. 2009.
- [42] G. Peyré, "Best basis compressed sensing," in *Proc. SSVM*, Jun. 2007, pp. 80–91.
- [43] E. Le Pennec and S. Mallat, "Sparse geometrical image approximation with bandlets," *IEEE Trans. Image Process.*, vol. 14, no. 4, pp. 423–438, Apr. 2005.

- [44] J. Raja, B. Muralikrishnan, and S. Fu, "Recent advances in separation of roughness, waviness and form," *Precis. Eng.*, vol. 26, no. 2, pp. 222–235, Apr. 2002.
- [45] L. Rudin, S. Osher, and E. Fatemi, "Nonlinear total variation noise removal algorithm," *Phys. D*, vol. 60, no. 1–4, pp. 259–268, Nov. 1992.
- [46] R. Scott, P. Ungar, T. Bergstrom, C. Brown, F. Grine, M. Teaford, and A. Walker, "Dental microwear texture analysis shows within-species diet variability in fossil hominins," *Nature*, vol. 436, no. 7051, pp. 693–695, Aug. 2005.
- [47] J. L. Starck, E. J. Candès, and D. L. Donoho, "The curvelet transform for image denoising," *IEEE Trans. Image Process.*, vol. 11, no. 6, pp. 670–684, Jun. 2002.
- [48] J. A. Tropp and A. C. Gilbert, "Signal recovery from random measurements via orthogonal matching pursuit," *IEEE Trans. Inf. Theory*, vol. 53, no. 12, pp. 4655–4666, Dec. 2007.
- [49] L. Villemoes, "Wavelet packets with uniform time–frequency localization," *C. R. Acad. Sci. Paris*, vol. 335, no. 10, pp. 793–796, Nov. 2002.
- [50] D. J. Whitehouse, "Surface metrology," *Meas. Sci. Technol.*, vol. 8, no. 9, pp. 955–972, Sep. 1997.
- [51] J. Xu and S. Osher, "Iterative regularization and nonlinear inverse scale space applied to wavelet based denoising," *IEEE Trans. Image Process.*, vol. 16, no. 2, pp. 534–544, Feb. 2007.



**Jianwei Ma** received the Ph.D. degree in solid mechanics from Tsinghua University, Beijing, China, in 2002.

He has been a Visiting Scholar, Research Fellow, Postdoctoral Scientist, and Guest Professor with the University of Cambridge, Cambridge, U.K., the University of Oxford, Oxford, U.K., the University of Huddersfield, Huddersfield, U.K., the University of Mannheim, Mannheim, Germany, Institut National de Recherche en Informatique et Automatique (INRIA), Paris, France, and the University of Duisburg-Essen, Duisburg-Essen, Germany. Since 2006, he has been an Assistant Professor with the School of Aerospace, Tsinghua University. From June to August 2006, he was a Visiting Professor with the Swiss Federal Institute of Technology (EPFL), Lausanne, Switzerland. From June to September 2007, he was a Visiting Professor with Florida State University, Tallahassee, FL, and the University of Colorado, Boulder. In May 2008, and from March to September 2009, he was an Invited Professor with INRIA-Grenoble and Ecole des Mines de Paris, Fontainebleau, France. He is an Editor of the *International Journal of Artificial Intelligence*. He is the author or a coauthor of about 40 papers in refereed journals. His research interests include wavelets, curvelets, image processing, compressed sensing, surface metrology, aerospace remote sensing, and seismic exploration.